

ABSTRACT

Raymond S. Lyon Jr. *Hox* Gene Expression During *Oreochromis niloticus* Pharyngeal Arch Development: Discovering The Hox Code. (Under the direction of Dr. Jean-Luc Scemama)
Department of Biology, January 2010.

Hox genes encode transcription factors and have been extensively studied by evolutionary and developmental biologists. *Hox* genes are responsible for determining specific regional identities along the anterior-posterior and proximal-distal developmental axes. Multiple *hox* genes are often simultaneously expressed in a developing tissue. Understanding the spatial and temporal expression patterns of the *hox* genes involved in morphogenesis is therefore essential for the prediction of molecular mechanisms that direct morphogenesis and patterning. The combinatorial *hox* gene expression (spatial and temporal) within a defined compartment is dubbed the “hox code.”

This study investigated the spatial and temporal expression of paralogous group 3-6 *hox* genes expressed within the pharyngeal arches of *Oreochromis niloticus* (Nile tilapia) embryos. It was hypothesized that each pharyngeal arch of Nile tilapia developing embryos would have a distinct combinatorial code of *hox* gene expression. The data shows that while pharyngeal arch 3 expresses *hoxa2a* and *hoxa3a* genes, pharyngeal arch 4 expresses *hoxd3a* and *hoxd4a* in addition to *hoxa2a* and *hoxa3a*. Pharyngeal arch 5 continues to express the *hox* genes found within pharyngeal arches 3 and 4, as well as *hox* genes *b3b*, *b4a*, and *d4b*. *Hox* expression within pharyngeal arch 6 is more diverse than the previous arches. In pharyngeal arch 6, all the *hox* genes expressed in pharyngeal arch 5 are present, with the following notable exceptions: *hox* genes *d3a* and *d4b* are excluded, and *hox* genes *a4a*, *a5a*, and *b5a* are included. Lastly, pharyngeal arch 7 is host to numerous expressed *hox* genes. The expression in pharyngeal arch 7 is similar to that of pharyngeal arch 6, having lost only *hoxb3b*. Four *hox* genes, *hox c4a*, *b5b*,

b6a, and b6b, have anterior pharyngeal expression limits that begin in pharyngeal arch 7. Our results clearly demonstrate that within each pharyngeal arch is expressed a unique combination of *hox* genes, or pharyngeal hox code.

***Hox* Gene Expression During *Oreochromis niloticus* Pharyngeal Arch Development:
Discovering the Hox Code**

A Thesis

Presented to

The Faculty of the Department of Biology

East Carolina University

In Partial Fulfillment

Of the Requirements for the Degree

Master of Science in Molecular Biology and Biotechnology

by:

Raymond Stewart Lyon Jr.

January 2010

©Copyright 2010
[Raymond Stewart Lyon Jr.]

Hox Gene Expression during *Oreochromis niloticus* Pharyngeal Arch Development:

Discovering the Hox Code

By

Raymond Stewart Lyon Jr.

DIRECTOR OF THESIS _____
Jean Luc Scemama, Ph.D

COMMITTEE MEMBER _____
Anthony Capehart, Ph.D

COMMITTEE MEMBER _____
Isabelle Lemasson, Ph.D

COMMITTEE MEMBER _____
Edmund Stellwag, Ph.D

CHAIR OF THE DEPARTMENT OF BIOLOGY _____
Jeffrey, McKinnon, Ph.D

DEAN OF THE GRADUATE SCHOOL _____
Paul Gemperline, Ph.D

ACKNOWLEDGEMENTS

My journey towards completing this thesis project has been ameliorated by the guidance, support, encouragement, and inspiration offered by many members of our department. It is with sincere gratitude that I acknowledge those contributions.

I would first like to express my thanks to Dr. Jean Luc Scemama. I believe his assistance throughout my graduate student experience has transcended his obligations. The time I have spent working as a member of his laboratory has been truly valuable and memorable.

Thanks are also extended to Dr. Pierre Le Pabic, without him this project may not exist! His research with the Nile tilapia has been astounding and productive. His guidance in all details of my experiment, from fundamental care of the fish to specific technical advice, has been tremendously appreciated.

Special thanks are given to Dr. Terry West; I feel he has been an advocate and mentor to me. Without his encouragement and guidance, it is unlikely that I would have been as successful as a graduate student.

I am also thankful for the efforts of the entire committee. The collective support and cooperation I have received from the committee has been remarkable.

Finally, I am thankful to all my friends and family. The encouragement and support they have offered on a personal level has often reaffirmed my ambition. Their presence in my life has made this experience enjoyable and absolutely unforgettable.

TABLE OF CONTENTS

CHAPTER 1: INTRODUCTION.....	1
CHAPTER 2: MATERIALS AND METHODS.....	11
CHAPTER 3: RESULTS.....	24
CHAPTER 4: DISCUSSION.....	33
REFERENCES.....	44
APPENDIX A: Supporting Information for Materials and Methods.....	48
APPENDIX B: Additional Images from <i>In Situ</i> Hybridization.....	66
APPENDIX C: Approval of Research Involving Animals.....	68

CHAPTER 1: INTRODUCTION

Hox genes were first discovered by Ed Lewis, who stumbled upon a series of most intriguing mutations in *Drosophila melanogaster*. The mutations, curiously positioned in a similar region of the chromosome, were able to cause complete morphological displacement of major anatomical features. With the mutation of a single gene, Lewis was able to observe legs develop in the head of *D. melanogaster*, in the place of antennae (Lewis 1978). Such transpositions were later dubbed “homeotic transformations”.

It is now understood that the genes Ed Lewis was observing were the *D. melanogaster* equivalent to homeobox containing *hox* genes (Krumlauf 1994). These genes, found across all vertebrate species, are quintessential among those genes regulating development. Although vertebrate *hox* genes are much more abundant in number than in invertebrates, *hox* genes have been shown to be amazingly conserved in terms of chromosomal organization, pattern of physical expression, and general molecular function among all *hox* containing life forms (Gaunt 1994; Wagner et al. 2003).

Hox genes encode transcription factors, the hallmark of which is the homeodomain, a 60 amino acid helix-turn-helix protein motif which directly binds to genomic DNA at sequence specific enhancer sites (Krumlauf 1992). *Hox* genes thus act as super-regulators of development, activating or repressing the transcription of multiple downstream target genes, ultimately orchestrating morphogenesis and segmental specification in the developing embryo (Gilbert 2000).

The downstream target genes of the *D. melanogaster* homeotic complex genes have been identified (Vachon et al. 1992; Mastick et al. 1995; Capovilla et al. 1998; Lohmann et al. 2002). Among the *D. melanogaster* downstream genes targeted by homeotic complex genes are the

genes *distal-less*, *decapentaplegic*, *reaper*, and *dapentaplegic* (Vachon et al. 1992; Mastick et al. 1995; Capovilla et al. 1998; Lohmann 2003). Research into the downstream target genes of vertebrate *hox* genes, however, has not been as productive. The task of elucidating the downstream targets of *hox* genes is complicated due to the larger number of genes in vertebrate genomes. The homeodomain of *hox* genes are known to recognize and bind to the “TAAT” sequence on genomic DNA (Knoepfler et al. 1996). Because this is such a short recognition sequence, a large number of downstream targets are theoretically possible. The *hox* genes are known to achieve target specificity *in vivo* via recruitment of cofactors (Mann et al. 2009). The Meis homeodomain proteins have been shown to bind the Pbx protein to *hox* genes (Choe et al. 2002). This complex of proteins then interacts with genomic DNA to regulate target gene expression. These cofactors have been shown to be critical for development. Not surprisingly, murine Meis and Pbx loss of function studies result in phenotypes similar to those found in mice lacking *hox* paralogous group 1 and 2 genes (Choe et al. 2002).

Perhaps the most elegant and mysterious feature of the *hox* genes is the concept of colinearity. Paralogous groups 1-13 are found in numerically ascending order along the chromosome in the order of transcription (3' to 5'). Astoundingly, the *hox* paralogous groups have been shown to be spatially and temporally expressed in ascending order along the anterior-posterior axis (Duboule 1998). Thus, the location of a *hox* gene on a chromosome is “colinear” with its pattern of expression (Krumlauf 1994).

Hox clusters are thought to have initially developed by way of tandem duplications of a few ancestral homeobox containing genes in an ancestral invertebrate species (Patel et al. 2000). The tandem duplication events resulted in neofunctionalized coding regions, although the precise mechanism is poorly understood. Current supported theories state that newly segmented

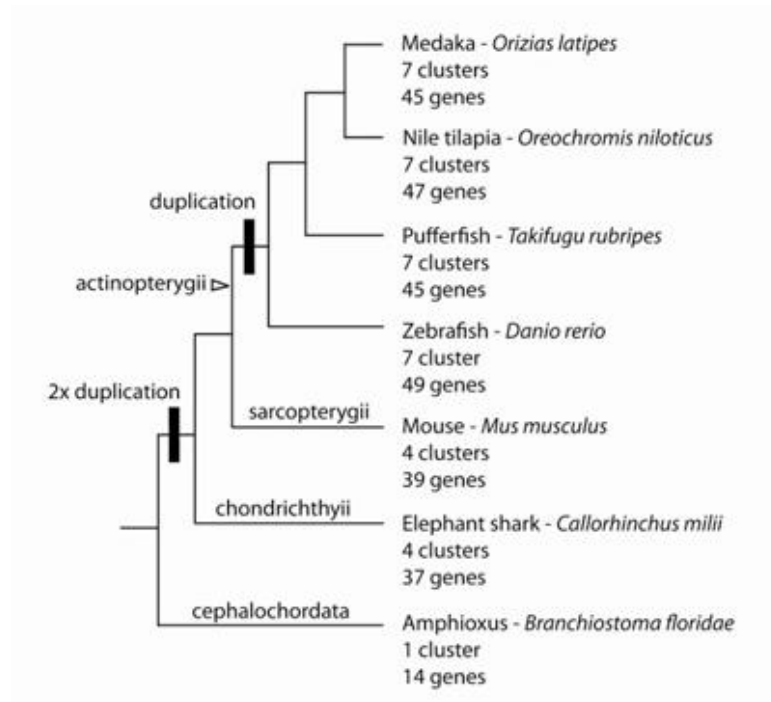
duplicated genes could experience mutations or inherit variable enhancer elements, thereby altering gene expression patterns. Exon shuffling, generation of alternative transcripts, and the evolution of novel enhancer elements are also supported theories of *hox* cluster evolution (Patel et al. 2000).

It has been accepted that vertebrate *hox* clusters do not undergo tandem duplications, despite their original invertebrate genesis via tandem duplication. Vertebrate *hox* clusters appear to be constrained, thereby protecting them from common forces that would otherwise drive evolution and divergence (Wagner et al. 2003). Vertebrate *hox* clusters are instead thought to be vulnerable to such mechanisms shortly after a genome or chromosomal doubling event, providing a short window of opportunity for genetic diversity to arise (Chiu et al. 2000; Van de Peer et al. 2001).

Because vertebrates have a minimum of four distinct *hox* clusters, it is obvious that some mechanism other than ancestral tandem duplication occurred, thereby increasing the total number of *hox* clusters. This mechanism is known to be a series of genome duplications, although there are competing theories dictating the precise number and timing of such genomic duplication events (Hughes 1999). It is accepted, however, that at least two genomic duplication events occurred which gave rise to four distinct *hox* clusters in ancient gnathostome (jawed vertebrate) species (Ohno 1970; Furlong et al. 2004).

The genomic duplications did not end with the gnathostome event. It has been discovered that teleost actinopterygians have seven *hox* clusters (Amores et al. 1998). Phylogenetic investigations revealed that another genomic duplication specific to the teleostean species occurred, resulting in eight *hox* clusters (Taylor et al. 2003; Jaillon et al. 2004). The duplication event was followed by the loss of a *hox* cluster, resulting in the current genomic

condition of seven *hox* clusters (Santini et al. 2005). The duplication events are illustrated in the phylogenetic map shown below.



***Hox* gene complement evolution in Osteichthyyii.** Phylogeny of osteichthyan *Hox* clusters.

(Phylogenies based on Steinke et al., 2006, figure from Le Pabic, 2009).

A uniform system of nomenclature has been adopted to simplify scientific communication concerning *hox* genes (Scott 1993). A *hox* gene is first identified by the letter of the *hox* cluster to which it belongs (A-D). The paralogous group to which it belongs is then listed (1-13). Due to the genomic duplication event specific to the teleost evolutionary radiation, letters “a” and “b” are used to distinguish copies of *hox* genes in teleosts.

The Nile tilapia is a teleost and an actinopterygian (ray-finned) fish. Ray-finned fish compose more than 50% of all vertebrate species and are therefore excellent model organisms for developmental studies in vertebrate organisms (Hoegg et al. 2007). Furthermore,

actinopterygians are a phenotypically diverse group despite their close evolutionary lineage. Not surprisingly, changes in the genomic complement of *hox* genes have been implicated to play a role in causing the aforementioned actinopterygian diversity (Hurley et al. 2005). The genome of *Oreochromis niloticus* will soon be entirely mapped and is currently known to contain seven *hox* clusters, not four as in mammals and other vertebrates due to the teleostean genomic duplication as previously described (Hurley et al. 2005). The *hox* cluster Cb has been lost; this is similar to other teleosts, with the major exception being *Danio rerio*, which has instead lost *hox* cluster Db.

Hox cluster number appears stable within teleost species; however *hox* gene complement within the clusters is variable. The *hox* gene complement of *Oreochromis niloticus* includes 47 *hox* genes. *O. niloticus* appears to have lost *hoxc1a* upon radiation, however the evolutionary loss of *hoxc1a* is not uniformly observed in other related species (Santini et al. 2005). The genomic *hox* complement signature of *Oreochromis niloticus*, separating it from its closest phylogenetic neighbor, *Astatotilapia burtoni*, is the presence of the *hoxb7a* gene which appears to be lost in *A. burtoni* (Hoegg et al. 2007).

Hox genes have most notably been discovered to regulate anterior-posterior patterning in developing vertebrate organisms. Murine genetic experiments have indicated that the specific combinatorial expression of *hox* genes is paramount to segmental identity and vertebral classification (Kessel et al. 1990; Wellik 2007). Independent knockdown of the *hox* 5, 6, 9, 10, and 11 groups produce dramatic phenotypes characterized by homeotic transformation of vertebral identity (Wellik 2007). For example, *hox* 10 knockout mice present a dramatic transformation of the lumbar and sacral vertebrae to a thoracic morphology, complete with small rib-like projections (Wellik et al. 2003). Clearly *hox* 10 in mice has a very specific role in

specifying vertebral identity, and is an important contributor to the combinatorial *hox* regulation within the somites. The combinatorial pattern of *hox* gene expression within a defined compartment is dubbed the “*hox* code” (Hunt et al. 1991). This data lent support to the existence of an axial *hox* code, implying that the combination of *hox* expression in a segment will direct its development.

The findings from these murine *hox* misexpression experiments were supported by a comparative study of somitic *hox* expression in both chicken and mouse (Burke et al. 1995). It was determined that vertebral identity (cervical, thoracic, lumbar, etc.) was marked by specific combinatorial patterns of *hox* expression (Burke et al. 1995). The number of each type of vertebrae was then implicated to be a cause of morphological diversity (Burke et al. 1995). These studies definitively illustrate the presence of a vertebrate *hox* code.

Knowing the *hox* code for various organisms is of great value to developmental biologists, as this provides insight into a fundamental mechanism of cell fate determination. Furthermore, available *hox* codes allow evolutionary and developmental biologists to begin understanding how such tremendous anatomical diversity arose in vertebrate lineages.

Known expression domains for *hox* genes in developing vertebrate embryos include the neural tube, paraxial mesoderm, and pharyngeal arches (Trainor et al. 2001). The expression of *hox* genes within the neural tube is not surprising, as *hox* genes have been implicated in participating in nervous system patterning and as previously discussed, anterior-posterior axis patterning (Trainor et al. 2000). *Hox* expression within the pharyngeal arches highlight the possible important role these genes play in the specification of these structures (Schilling et al. 1994; Piotrowski et al. 1996; Schilling et al. 1996; Hunter et al. 2002; Minoux et al. 2009).

Data is accumulating which directly links combinatorial *hox* expression to pharyngeal arch identity. Up to seven pharyngeal arches give rise to key craniofacial elements in vertebrates. Several loss and gain of function experiments have been performed in tetrapods, examining the role of the *hoxa2* gene specifically. Mouse *hoxa2* null mutants are characterized by a transformation of the derived cartilages of the second pharyngeal arch (Gendron-Maguire et al. 1993; Rijli et al. 1993). These derived cartilages assume the morphological identity of cartilages naturally derived from the first pharyngeal arch (Gendron-Maguire et al. 1993). This implicates that *hoxa2* acts *in vivo* as a marker of second pharyngeal arch identity. *Hoxa2* knockdown in *Xenopus* produces a similar transformation of pharyngeal-derived cartilage identity (Baltzinger et al. 2005). Gain of function experiments for *hoxa2* further verifies the role of *hoxa2* as a selector gene for tetrapod pharyngeal arch 2 identity; *hoxa2* gain of function experiments in chicken and *Xenopus* result in a transformation of first pharyngeal arch derived cartilages to that of second pharyngeal arch derived cartilages (Grammatopoulos et al. 2000; Pasqualetti et al. 2000).

The role of *hoxa2* in determining the second pharyngeal arch identity is not specific to tetrapods. Knockdown of *hoxa2b* and *hoxb2a* in the teleost *Danio rerio* results in a phenotype similar to that found in the previously mentioned tetrapod *hoxa2* loss of function studies, in which the derived cartilages of the second pharyngeal arch take on the morphology of the cartilages derived from the first pharyngeal arch (Hunter et al. 2002).

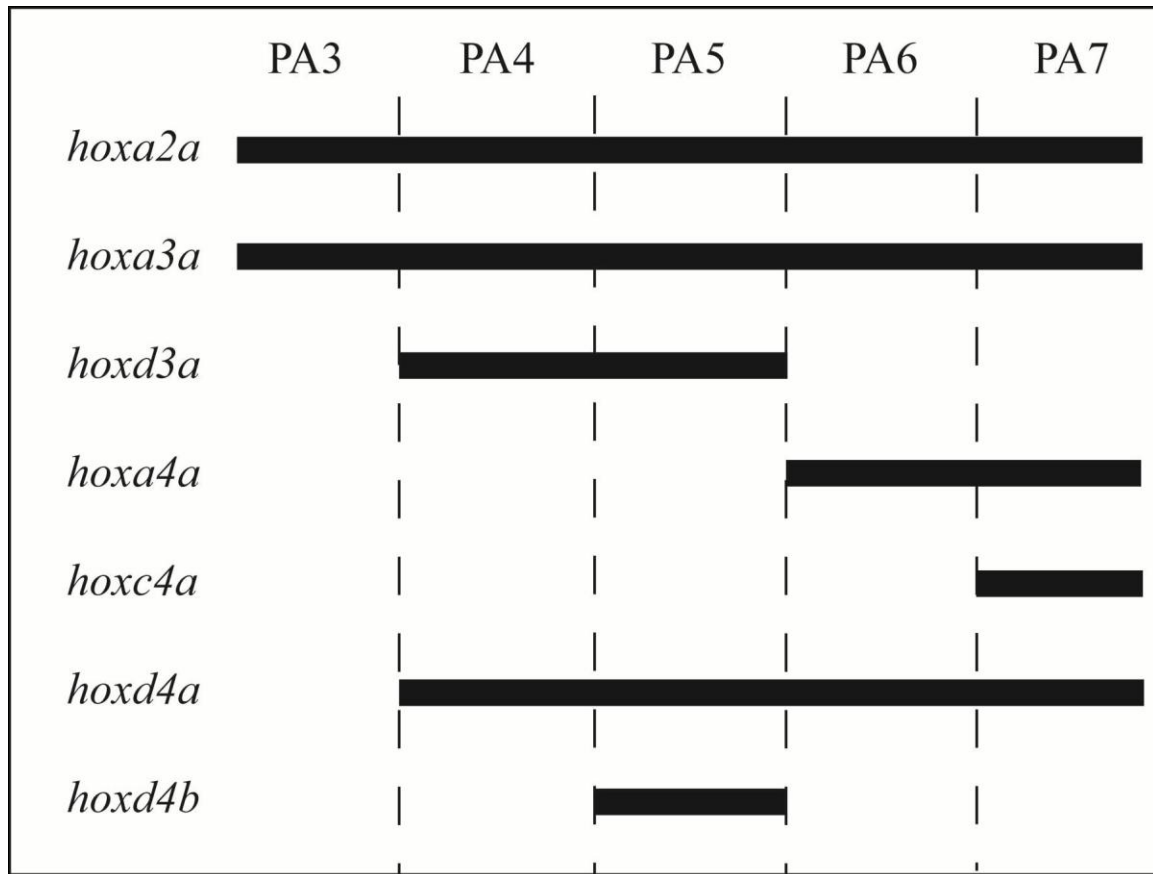
In teleosts, the first pharyngeal arch gives rise to the lower jaw apparatus, while the remaining pharyngeal arches give rise to skeletal elements of the jaw and gills, including the suspensorium, gill arch, and pharyngeal jaw apparatus (PJA).

Preliminary research gathered in our lab suggests that each pharyngeal arch of *Oreochromis niloticus* is characterized by a specific combinatorial *hox* expression complement, which we have dubbed the “pharyngeal *hox* code.” Several lines of evidence have led us to this hypothesis. The posterior arches of tilapia have very different morphologies, which could easily be explained by variation in their *hox* codes, if such codes were shown to exist (Le Pabic et al. 2009). Studies from our lab and others also indicate that no *hox* genes are expressed within the first pharyngeal arch (Le Pabic et al. 2007). Curiously, *hox* paralogous group 2 genes are the only *hox* genes expressed within the second pharyngeal arch (Le Pabic et al. 2007). A loss of function study of the *hoxa2a*, *hoxa2b*, and *hoxb2a* genes of *O. niloticus* embryos produced phenotypes consisting of the loss of second pharyngeal arch derived cartilages; the cartilages transformed into morphologies consistent with those derived from the first pharyngeal arch. Independent morpholino knockdown of all three *hox* paralogous group 2 genes resulted in this phenotype. Furthermore, and perhaps most striking, the loss of function study also produced a phenotype consisting of the presence of a supernumerary arch, as defined by an extra set of hypo-, cerato-, and epi-branchial cartilages. This data definitively shows a function for *hox* paralogous group 2 genes in determining the molecular identity of the *O. niloticus* pharyngeal arches.

The *O. niloticus* *hox* expression within the posterior arches, arches 3-7, has not been fully investigated. The expression of approximately one-half of the *hox* genes in paralogous groups 3-6 have been analyzed, and the data continues to suggest that there is indeed a combinatorial pharyngeal *hox* code as each pharyngeal arch expresses different combinations of *hox* genes (Le Pabic et al. 2009). The figure below illustrates this combinatorial expression data previously gathered for *hox* genes within the pharyngeal arches of developing *O. niloticus* embryos.

This study will analyze the expression of the eight remaining paralogous group 3-6 *hox* genes: b3b, c3a, b4a, a5a, b5a, b5b, b6a, and b6b. This range of paralogous groups has been selected because it will encompass the expected *hox* expression within pharyngeal arches of developing embryos (Le Pabic et al. 2007). The *in situ* hybridizations will be performed on embryos at the following time points: 42 hpf, 48 hpf, 54 hpf, 60 hpf, 66 hpf, and 72 hpf. These time points encompass the mid-segmentation to late pharyngula *Oreochromis niloticus* developmental stages, coinciding with pharyngeal arch formation (Le Pabic et al. 2009).

The pharyngeal *hox* code of *Oreochromis niloticus* will be compiled using this new data as well as the expression data previously generated in our lab. It is hypothesized that each pharyngeal arch of developing embryos will have a distinct combinatorial code of *hox* gene expression. To our knowledge, no study investigating the existence of a pharyngeal *hox* code has been performed. Discovering a pharyngeal *hox* code would implicate a novel mechanism of morphological determination. The data obtained from this study will lend foundational information necessary for future developmental and evolutionary studies, including but not limited to those concerning the family Cichlidae.



Combinatorial code of *hox* expression in Nile tilapia posterior pharyngeal arches at 60hpf.

(Le Pabic et al. 2009)

CHAPTER 2: MATERIALS AND METHODS

A. Embryo Incubation and Collection

Nile tilapia adults (*Oreochromis niloticus*) were observed during spawning activity. The precise time of fertilization was recorded as determined via physical observation. Following fertilization, the embryos were allowed to develop in the mother fish's mouth for 24 hours. At 24 hours post-fertilization, the embryos were physically removed from the mother fish's mouth and transferred to Macdonald jars filled with sterilized aquarium system water (28° C). Water flow into the Macdonald jars allowed for gentle agitation of the embryos, simulating the developmentally important movements naturally occurring in the mother fish's mouth. The embryos were allowed to develop until time of sampling. Upon sampling, the embryos developmental stages were verified using established staging protocols (Fujimura et al. 2007; Le Pabic et al. 2009).

B. Embryo Preservation

Staged embryos were quickly euthanized by immersion in MS-222 (0.04%, w/v) and transferred to 50 mL conical tubes where they were fixed for 7 days via immersion in 4 % paraformaldehyde in phosphate-buffered saline (PBS) at 4° C (five volumes PFA to 1 "volume" embryos), conditions determined to provide the best signal-to noise ratio in the whole-mount in situ hybridization experiments (Le Pabic et al. 2007).

Following the fixation period, the excess PFA was removed. The embryos were dehydrated via a series of methanol/PBT washes of increasing methanol concentration. Concentrations of methanol used include 25%, 50%, 75%, and 100%. (v/v). Two 10-minute

washes at each concentration of methanol/PBT were performed. Embryos were stored in absolute methanol at -20°C until needed for further use.

C. RNA Extraction and cDNA Synthesis

Total RNA was isolated from live *O. niloticus* embryos at the following developmental time points: 30 hpf, 50 hpf, 64 hpf, and 72 hpf. The total RNA was isolated using Ambion, Inc.'s kit "Totally RNA" (Ambion, Foster City, CA). The RNA was analyzed for concentration, purity, and integrity via spectrophotometry and gel electrophoresis. Complimentary DNA (cDNA) was synthesized from the extracted total RNA using SuperScript® III First-Strand Synthesis System (Invitrogen, Grand Island, NY).

D. Molecular Cloning

PCR primer sets specific for each of the *hox* genes b3b, c3a, b4a, a5a, b5a, b5b, b6a, b6b were designed using Vector NTI software (Invitrogen, Grand Island, NY). Sequence information was obtained from NCBI using published sequence data for both *Oreochromis niloticus* and the close phylogenetic relative *Astatotilapia burtoni*. Accession numbers can be found in Appendix A-Table 1. The primers were designed using sequences from the *O. niloticus* genome, and in cases of incomplete *O. niloticus* sequences, the *A. burtoni* genome. PCR primer sets, PCR conditions, and expected amplicons can all be found in Appendix A-Table 2. The cDNA generated from the RNA extracted from the time points previously listed was pooled. The pooled cDNA was then used as template for PCR for each gene being investigated. The PCR products were analyzed on agarose gel electrophoresis. Images of

cDNA amplifications are found in Appendix A-Figure 1A-1D. The following PCR reaction was used:

PCR

10 x PCR Buffer	5 μ l
50 mM MgCl ₂	1.5 μ l
10 mM dNTP	1.0 μ l
Taq Polymerase	0.5 μ l
Forward Primer (3 pmol/ μ l)	5 μ l
Reverse Primer (3 pmol/ μ l)	5 μ l
Sterile distilled water (SDW)	31 μ l
cDNA	1 μ l

The PCR products were each cloned into the pCRII vector (TA Cloning Kit-Dual Promoter pCRII, Invitrogen). The ligation reaction is found below.

pCRII Dual Promoter Ligation Reactions

PCR Product	5 μ l
10 x Reaction Buffer	1 μ l
T ₄ DNA Ligase	1 μ l
pCRII Vector	2 μ l
SDW	1 μ l

The reactions were incubated overnight at 14° C, according to manufacturer's instructions. The ligated product was stored at -20° C until needed for further use.

Following ligation, *E. coli* of strain JM-109 were made chemically competent in preparation for transformation with the recombinant plasmids. Cells from a small, fresh, colony were aseptically transferred to a 15 mL conical tube containing 5 mL of sterile SOB. The tube was transferred to a 37° C shaking incubator and incubated overnight. Following the overnight incubation, 40 mL sterile SOB was added to an autoclaved side-armed 300 mL

flask. The SOB in the side-armed flask was inoculated with 500 μ l from the *E. coli* overnight culture. A second side-armed flask was prepared, lacking bacteria, which served as a blank for the Klett colorimeter. Both flasks were incubated at 37° C until the inoculated sample reached a Klett value of 25 units. The cells were then transferred from the side-armed flask to a sterile 50 mL conical tube and placed on ice for 15 minutes. Then the cells were centrifuged at 2500 rpm for 12 minutes at 8° C. The supernatant was decanted, and the bacterial pellet resuspended in transformation buffer (TFB), using an amount of TFB corresponding to 1/3 of the original volume of the cellular suspension. The cells were incubated on ice for 15 minutes.

The cells were once again centrifuged and the supernatant was decanted. The bacterial pellet was then resuspended in (TFB), using an amount of TFB corresponding to 1/12.5 of the original volume of the cellular suspension. The resuspension was aliquoted to microcentrifuge tubes (200 μ l each). Seven microliters of fresh DMSO (RT) was added to each aliquot of cells to give a final concentration of 3.5% (v/v) DMSO. The tubes were flicked gently to mix. The tubes were incubated on ice for 5 minutes. Seven microliters of stock DTT (75 mM final concentration) was then added to each of the tubes, and incubated on ice for 10 minutes. Finally, 7 μ l of fresh DMSO was again added to each tube. The tubes were mixed and placed on ice for 5 minutes.

The cells were then transformed using the previously generated plasmids (frozen ligation products). Five microliters of the appropriate recombinant plasmid was added to its respective microcentrifuge tube of chemically competent bacterial cells. A positive control tube was utilized, containing pUC19 plasmid. A negative control tube was utilized, lacking any plasmid. After the addition of plasmid, the tubes were mixed gently and placed on ice

for 30 minutes. Following incubation, the tubes were heat shocked for 45 seconds in a 42° C water bath. Immediately following the water bath incubation, the tubes were placed back onto ice, and 800 µl SOC medium was added to each tube. The tubes were then placed in a shaking incubator, and incubated at 37° C, 225 rpm, for 60 minutes. 150 µl of each tube was then aseptically pipette and plated onto its respectively labeled XIA plate (X-gal, IPTG, and ampicillin). Plates were inverted and incubated at 37° C overnight.

Transformant bacterial colonies were selected via blue-white screening. White colonies were selected, indicating a successful transformation. The colonies were cultured and the plasmids harvested and purified using a miniprep kit (Sigma-GenElute Plasmid Miniprep Kit) according to the manufacturer's instructions, with the exception that the plasmid was eluted in SDW. Insert size was verified by digesting the recombinant plasmid with the EcoRI endonuclease which allow for complete cleavage of the insert. The EcoRI restriction enzyme reactions were prepared are follows, and were incubated at 37° C for two hours.

EcoRI Digestion Reactions for Verification of Insert Identity

Purified Plasmid	7.0 µl
EcoRI Enzyme	1.0 µl
React 3 Buffer	1.0 µl
SDW	2.0 µl

The results of the restriction digests were analyzed using agarose gel electrophoresis (Appendix A-Figure 2: A-D). Plasmids containing the appropriate insert were quantified using a nanodrop spectrophotometer (Appendix A-Table 3). Plasmid preps containing inserts of expected size were sent for dideoxynucleotide sequencing in the Genomic core facility and

their identity checked by comparison with sequences available in the GeneBank database and more specifically were compared to *O. niloticus* and *A. burtoni* genomes (Appendix A-Figure 3). The insert orientation for each of the recombinant plasmids was determined using the sequence data comparisons (Appendix A-Table 4).

E. Riboprobe Construction

The sequences of the plasmids and inserts were analyzed using New England Biolabs' NEBcutter V2.0, in order to determine the appropriate restriction enzymes to use for linearization of the plasmids. Restriction enzymes were selected based on the following criteria: location of the restriction site in the polycloning site and absence of restriction site in the insert (plasmid map found in Appendix A-Figure 5). Restriction enzymes selected can be found below.

Restriction Enzymes For Plasmid Linearization

Plasmid Name	To Form Antisense Probe	To Form Sense Probe
B3b-c	Xho1	Spe1
C3a-b	Xho1	Spe1
C3a-c	Xho1	Spe1
B4a-2	EcoRV	Spe1
A5a-c	Spe1	Xho1
B5a-2-1	EcoRV	BamH1
B5b-2	Xho1	Spe1
B6a-1	Spe1	EcoRV
B6a-3	EcoRV	Spe1
B6b-3	Xho1	Spe1

Restriction enzyme digestion reactions were prepared using the selected enzymes. The reactions were prepared as found below. The linearization reactions were incubated at 37° C for 2.5 hours. The reactions were then purified via Qiagen's Minelute Purification kit according to manufacturer's instructions (Qiagen, Valencia, CA). Gel electrophoresis was then performed using an aliquot of purified DNA to ensure that linearization had occurred and was complete.

Plasmid Linearization Restriction Enzyme Digestions Reactions

Plasmid	5 µg= ____ µl
10x Buffer	15 µl
Restriction Enzyme	2 µl
dH ₂ O	Fill to 150 µl

Digoxigenin labeled sense and antisense RNA probes were then prepared using Ambion's Maxiscript transcription reaction kit. SP6 and T7 enzymes were used; the specific enzyme used being dependent upon insert orientation. The enzymes used as well as the transcription reactions are shown below:

Enzymes Used for Transcription Reactions

Plasmid Name	Enzyme for Sense Strand	Enzyme for Antisense Strand
B3b-c	T7	Sp6
C3a-b	T7	Sp6
C3a-c	T7	Sp6
B4a-2	T7	Sp6
A5a-c	Sp6	T7
B5a-2-1	T7	Sp6
B5b-2	T7	Sp6
B6a-1	Sp6	T7
B6a-3	T7	Sp6
B6b-3	T7	Sp6

Transcription Reactions Synthesizing Antisense and Sense Probes

Linearized Plasmid	1 μ g = 5 μ l
10x Buffer	2 μ l
10x Digoxigenin Label	2 μ l
Enzyme (T7/Sp6)	2 μ l
DEPC-H ₂ O	Fill to 20 μ l

The transcription reactions were incubated for 1.5 hours at 37° C. Following the incubation, 1 μ l Turbo DNase was added to reach reaction. The reactions were then incubated at 37° C for an additional 15 minutes, allowing for complete digestion of plasmid DNA. The transcription reaction products were then purified using Qiagen's Minielute Purification kit according to manufacturer's instructions. The RNA was eluted from the columns using 20 μ l DEPC-H₂O. The volume of the RNA samples was then adjusted to 50 μ l each using DEPC-H₂O. Riboprobe quality was verified via gel electrophoresis, using 1.5 μ l of each RNA sample. The RNA probes were then immediately stored at -80° C until needed for later use.

Riboprobe concentrations were measured via dot blot against a control digoxigenin-labeled RNA (Roche). Using a pencil, a grid was set up on nylon filter paper. A plastic container to contain the nylon paper was decontaminated using RNase Erase. Dilutions in RNA dilution buffer (5 volumes DEPC-H₂O, 3 volumes 20x SSC, 2 volumes formaldehyde) of each of the riboprobes to be quantified were prepared, at the following dilutions: 1/5, 1/10, 1/50, 1/100, 1/200. The control DIG-RNA was also diluted. One μ l of each dilution was added to the appropriate grid position of the nylon filter paper. The RNA was crosslinked to the nylon filter using the Stratalinker (optimal crosslinking function). The filter was then incubated with 2X SSC for 10 minutes. The filter was then washed twice with PBT (10

minutes each). Following the PBT washes, the filter was “preincubated” for 1 hour with PI buffer. The filter was then incubated with digoxigenin (DIG) antibody (1/5000 dilution) in PI buffer for 30 minutes. Two more PBT washes followed, 10 minutes each. DIG/AP Buffer containing NBT and BCIP was then applied to the nylon filter and incubated on a nutator for 10 minutes. The filter was then washed twice with PBT (10 minutes each). The development was stopped by a quick wash with 4% PFA. The filter was then analyzed to determine the approximate concentration of the riboprobes.

F. Preparing Embryos for *In Situ* Hybridization

Previously dehydrated *Oreochromis niloticus* embryos stored at -20° C in absolute methanol, were poured into a standard petri dish. Using small forceps, a small scalpel, and a dissecting needle, the embryos were manually dechorionated under the magnification of a dissecting scope. The embryos were also carefully separated from the yolk. Extreme caution was used to ensure that the embryo was not damaged in the dechoriation/de-yolking process. The processed embryos were moved to microcentrifuge tubes, labeled with the corresponding developmental age of the embryos. The microcentrifuge tubes were filled with absolute methanol.

Following dechoriation and de-yolking, the dehydrated embryos were rehydrated via a series of methanol/PBT washes of decreasing methanol concentration. Concentrations of methanol used include 100%, 75%, 50%, and 25%. Each methanol/PBT wash occurred for 10 minutes on a plate shaker at room temperature. The 25% methanol/PBT solution was then removed and replaced with PBT. The embryos were incubated on a plate shaker for 5

minutes. The PBT wash was repeated 3 times for a total of 4 PBT washes. The embryos were then immediately used for *in situ* hybridization-day 1.

G. Whole Mount *In Situ* Hybridization

Protocols for all solutions used for in situ hybridization are located in Appendix A-Table 5.

Rehydrated embryos were transferred to an appropriately labeled 48 well plate (Costar). Five embryos were placed into each well. The embryos were permeabilized using proteinase-K. Five μ l of proteinase-K (stock = 20 mg/ml) was added to 10 mL of PBT in a sterile 15-mL conical tube. Four hundred μ l of the proteinase-K/PBT solution was added to each well. The embryos were digested for 15 minutes (42 hpf embryos) or 20 minutes (48-72 hpf embryos). Following incubation, the proteinase-K solution was immediately discarded and digestion was stopped by adding room temperature 4% PFA. The embryos were incubated in the 4% PFA for 20 minutes at room temperature on a plate shaker. The 4% PFA was then removed and replaced with 400 μ l PBT, and washed on a plate shaker for 5 minutes at room temperature. The PBT wash was then repeated three times for a total of four washes. The PBT in the wells was discarded and replaced with 400 μ l of pre-hybridization buffer, equilibrated to 70° C. The plate was placed incubated in a shaking hybridization oven at 70° C for 5 minutes. Following this short incubation, the pre-hybridization buffer was removed from each well and replaced with 400 μ l of fresh pre-hybridization buffer, equilibrated to 70° C. The plate was then placed in the 70° C shaking hybridization oven for 3 hours.

Prior to the end of the incubation with pre-hybridization buffer, sense and antisense riboprobes were added to appropriately labeled aliquots of hybridization buffer in sterile 15

mL conical tubes. Aliquot volume was calculated, allowing for each well utilized in the 48-well plate to receive 400 µl of the respected aliquot of hybridization buffer. One hundred ng of riboprobe was used per 300 µl hybridization buffer. Aliquots containing only hybridization buffer and no riboprobe were also prepared, serving as a negative “no probe” control.

Following the 3 hour incubation with pre-hybridization buffer, the buffer was discarded and replaced with 400 µl of the previously aliquoted hybridization buffer containing the appropriate riboprobe. The embryos were again placed in the 70° C shaking hybridization oven. The hybridization reactions were incubated for 16 hours.

Buffers A, B,C, 2X SSC, and 0.05X SSC were placed in the 70° C shaking oven to allow for equilibration. The 48-well plate was removed from the shaking oven and the hybridization buffer discarded. The embryos were then subjected to the following washing reactions listed in sequential order (400 µl of each buffer, 10 minutes each wash in the 70° C shaking hybridization oven): buffer A, buffer B, buffer C, 2X SSC, 0.05X SSC. The 0.05X SSC was removed from the wells and replaced with 400 µl of buffer D. The embryos were incubated in buffer D on a plate shaker at room temperature for 5 minutes. The embryos were then subjected to the following washing reactions listed in sequential order (400 µl of each buffer, 5 minutes per wash, room temperature on a plate shaker): buffer E, buffer F, PBT. The PBT was removed and replaced with 400 µl pre-incubation (PI) buffer equilibrated to room temperature. The embryos were incubated in the PI buffer for 1 hr at room temperature on a plate shaker.

During the PI buffer incubation, anti-DIG antibody was diluted to a 1:5000 concentration. The antibody was diluted using PI buffer. Following the 1 hour PI buffer incubation, the PI

buffer in the wells was discarded and replaced with 400 μ l of the 1:5000 diluted anti-DIG antibody solution. One well in the 48-well plate was designated as a “no antibody” negative control and therefore received only PI buffer (no antibody). The embryos were incubated on a plate shaker in a 4° C refrigerator overnight.

The anti-DIG antibody solution in the wells was discarded following overnight incubation, and replaced with 400 μ l PBT. The embryos were incubated at room temperature on a plate shaker for 15 minutes. This step was repeated 7 times to eliminate the unreacted excess antibody. The PBT from the eighth PBT was discarded and replaced with 400 μ l freshly prepared AP buffer. The embryos were incubated at room temperature on a plate shaker for 5 minutes. The AP buffer equilibration step was repeated twice more for a total of 3 AP buffer equilibration incubations. Fresh DIG/AP buffer containing NBT and BCIP was prepared and protected from light by wrapping the container (50 mL conical tube) with aluminum foil. The AP buffer in the wells was discarded and replaced with 400 μ l of the DIG/AP buffer containing NBT and BCIP. The 48-well plate was wrapped in aluminum foil to protect the developing reaction from light, and incubated on a plate shaker at room temperature. The progress of the development reactions was examined under a microscope at half hour intervals, as optimal development times varied among the different antisense riboprobes. Optimal development was subjectively determined, in order to minimize background coloration. As the development of embryos containing an antisense probe was stopped, the development of embryos containing the corresponding sense probe was also stopped. To stop the development once optimum development was reached, the DIG/AP substrate buffer in the wells containing that riboprobe was discarded and replaced with 400 μ l PBT, and washed for 5 minutes at room temperature. The PBT wash step was repeated 3

times for a total of 4 PBT washes. The PBT from the final PBT was removed and replaced with 600 μ l 4% PFA. The fixed embryos, still in the 48-well plate, were then refrigerated at 4° C until needed for mounting and imaging.

H. Embryo Mounting and Imaging

Embryos were individually removed from the 4% PFA and placed onto a labeled frosted microscope slide. A small drop of warmed 0.5% agarose was quickly placed directly onto the embryo. Using small forceps and a small dissecting prod, the embryo was quickly oriented in either a lateral or dorsal position. A glass cover slip was gently lowered onto the embryo. Microscopic analysis and digital imaging was then performed using Leica DMR microscope equipped with a Nikon D2x digital camera.

CHAPTER 3: RESULTS

The first step in the analysis of paralogous group 3-6 *hox* gene expression in Nile tilapia developing pharyngeal arches was the molecular cloning of the partial cDNAs corresponding to these genes. The cloned partial cDNAs were then used to synthesize the riboprobes utilized to perform *in situ* hybridization experiments.

Figure 1 shows the results of a typical RT-PCR amplification, in which three of the eight *hox* genes being investigated were amplified. Partial *hox* b3b, c3a, and a5a sequences were amplified from cDNA generated from various developmental time points (30 hpf, 50 hpf, and 72 hpf). While RT-PCR is not a quantitative technology, this experiment was performed to elucidate the kinetic of expression of these genes. As shown in Figure 1, the partial *hoxb3b* amplicon is detectable at 30 hpf. By 50 hpf, *hoxb3b* transcripts are represented by a very robust band while the level of transcript seems to decrease by 72 hpf, as indicated by a much less robust band compared to that of 50 hpf. The kinetic of expression of *hoxc3a* was found to assume a similar pattern of temporal occurrence. The *hoxc3a* transcripts are present at 30 hpf. The concentration of transcripts peak by 50 hpf, and quickly diminishes to nearly undetectable levels by 72 hpf. *Hoxa5a* transcripts were not found to be present at detectable levels at 30 hpf. In contrast to the previously discussed *hoxb3b* and *hoxc3a* genes, the *hoxa5a* gene is strongly expressed at 72 hpf.

The RT-PCR produced anticipated results, illustrating *hox* gene temporal colinearity of expression. *Hox* genes from a lower paralogous group (*hoxb3b* and *hoxc3a*) were detectable at earlier time points (30 hpf) than *hox* genes from a higher paralogous group (*hoxa5a*).

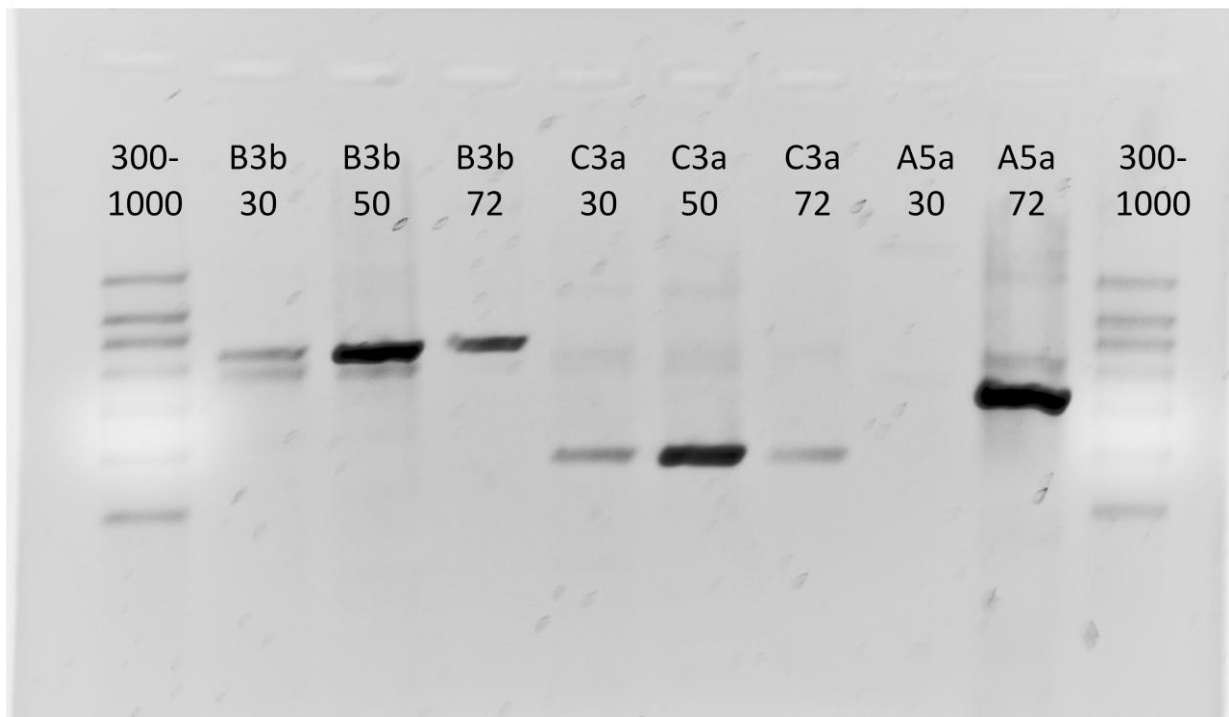
Figure 1: RT-PCR of Selected *Hox* Genes

Fig 1. RT-PCR of selected *hox* genes used to establish the kinetic of expression for *hox* genes b3b, c3a, and a5a. Image is the result of 1.5% gel electrophoresis of amplified cDNA. Lanes are labeled with the corresponding *hox* gene as well as the age of the embryo at time of RNA extraction and cDNA synthesis (30, 50, 72 hpf). The first and last lanes contain a synthesized DNA ladder, with bands ranging from 300 bp to 1000 bp in increments of 100 bp. The figure indicates that *hoxb3b* and *hoxc3a* transcripts are strongly expressed at 50 hpf. *Hoxa5a* is strongly expressed at 72 hpf.

Whole mount *in situ* hybridizations using antisense riboprobes were performed to identify the localizations of the investigated *hox* gene transcripts. *In situ* hybridizations using sense probes and no probe were performed as negative controls, and representative images from those controls are presented (Appendix B). The results for each investigated gene are described below, organized by corresponding *hox* paralogous group.

Paralogous Group 3

Hoxb3b (Figure 2) transcripts were detected within rhombomeres 4-7 at 42 hpf. No expression was found in any pharyngeal arch at 42 hpf. By 48 hpf, while expression persisted in rhombomere 4, we observed a reduction in transcripts from rhombomeres 5-7. *Hoxb3b* transcripts were shown to persist within rhombomere 4 at 54 hpf. *Hoxb3b* transcripts were first detected within the pharyngeal arches at 54 hpf, with its expression being localized within pharyngeal arches 5 and 6.

Hoxc3a (data not shown) transcripts were undetectable at any investigated time point in any location, despite the fact that we were able to amplify partial cDNA sequences corresponding to *hoxc3a* mRNA via RT-PCR (Figure 1). Multiple antisense riboprobes were designed to investigate the expression of *hoxc3a*. All antisense riboprobes used resulted in consistent lack of expression data.

Paralogous Group 4

Hoxb4a (Figure 2) transcripts were detected in pharyngeal arch 5 at 48 hpf. At this time point, light staining also occurred in rhombomere 7 and the immediately adjacent neural tube, indicating low yet detectable concentrations of *hoxb4a* transcripts. At 54 hpf, *hoxb4a* transcripts

were detected within pharyngeal arches 5 and 6, as well as the unsegmented tissue that would later form pharyngeal arch 7. Expression of *hoxb4a* within the neural tube intensified at 54 hpf. By 66 hpf, *hoxb4a* expression within the neural tube as well as expression in pharyngeal arch 5 had diminished to undetectable levels. At this time point, however, *hoxb4a* transcripts were found to persist within pharyngeal arch 6, and were also detected in the developed pharyngeal arch 7.

Paralogous Group 5

Hoxa5a (Figure 3) transcripts were first detected and localized with remarkable specificity to pharyngeal arches 6 and 7 at 66 hpf. Transcripts persisted within pharyngeal arches 6 and 7 at 72 hpf. At 72 hpf, transcripts were also detected within the anterior neural tube.

Hoxb5a (Figure 3) transcripts were detected within pharyngeal arches 6 and 7 at 66 hpf. At 72 hpf, expression in pharyngeal arch 6 diminished to a nearly undetectable level, but were present nonetheless. *Hoxb5a* transcripts also persisted within pharyngeal arch 7 at 72 hpf, although the staining in pharyngeal arch 7 was also less robust than at 66 hpf, suggesting that *hoxb5a* is transiently expressed within developing pharyngeal arches. *Hoxb5a* transcripts were not detected before 66 hpf (data not presented).

Hoxb5b (Figure 3) transcripts were present at a faint but detectable level within pharyngeal arch 7, and present at a readily detectable level within the anterior neural tube, at 66 hpf. At 72 hpf, *hoxb5b* transcripts persisted at a weak but detectable level within pharyngeal arch 7, and persisted at a readily detectable level within the neural tube. *Hoxb5b* transcripts were not detected before 66 hpf (data not presented).

Paralogous Group 6

Hoxb6a (Figure 4) transcripts were detected exclusively within pharyngeal arch 7 at 66 hpf. At 72 hpf, *hoxb6a* expression was not only maintained but increased within pharyngeal arch 7. At 72 hpf, *hoxb6a* transcripts were also detected within the neural tube. *Hoxb6a* transcripts were not detected before 66 hpf (data not presented).

Hoxb6b (Figure 4) transcripts were not detected in any location at 66 hpf. At 72 hpf, however, *hoxb6b* transcripts were readily observed within pharyngeal arch 7 and the neural tube.

The data presented here was added to the previously generated and published combinatorial expression data for *hox* genes within the pharyngeal arches of developing *O. niloticus* embryos (Le Pabic et al. 2009). Figure 5 merges and organizes the pharyngeal expression data, and summarizes the findings of this investigation. It was hypothesized that each pharyngeal arch of developing embryos would have a distinct combinatorial code of *hox* gene expression. This hypothesis has been fully supported, as illustrated below in Figure 5. It is known that pharyngeal arch 2 expresses only paralogous group 2 *hox* genes. Pharyngeal arch 3 has been shown to express *hox* genes a2a and a3a. Pharyngeal arch 4 expresses *hox* genes a2a, a3a, d3a, and d4a. Pharyngeal arch 5 continues to express members of *hox* paralogous groups 2-4. Specifically, pharyngeal arch 5 expresses *hox* genes a2a, a3a, d3a, b3b, b4a, d4a, and d4b. Pharyngeal arch 6 has been shown to express *hox* genes a2a, a3a, b3b, a4a, b4a, d4a, a5a, and b5a. Pharyngeal arch 7 expresses the most *hox* genes of all the arches, and is the only pharyngeal arch to express *hox* genes belonging to paralogous group 6. Pharyngeal arch 7 expresses *hox* genes a2a, a3a, a4a, b4a, c4a, d4a, a5a, b5a, b5b, b6a, and b6b.

Figure 2: Lateral Views of Whole Mount *In Situ* Hybridization: Antisense Probes of *Hox* Paralogous Groups 3-4

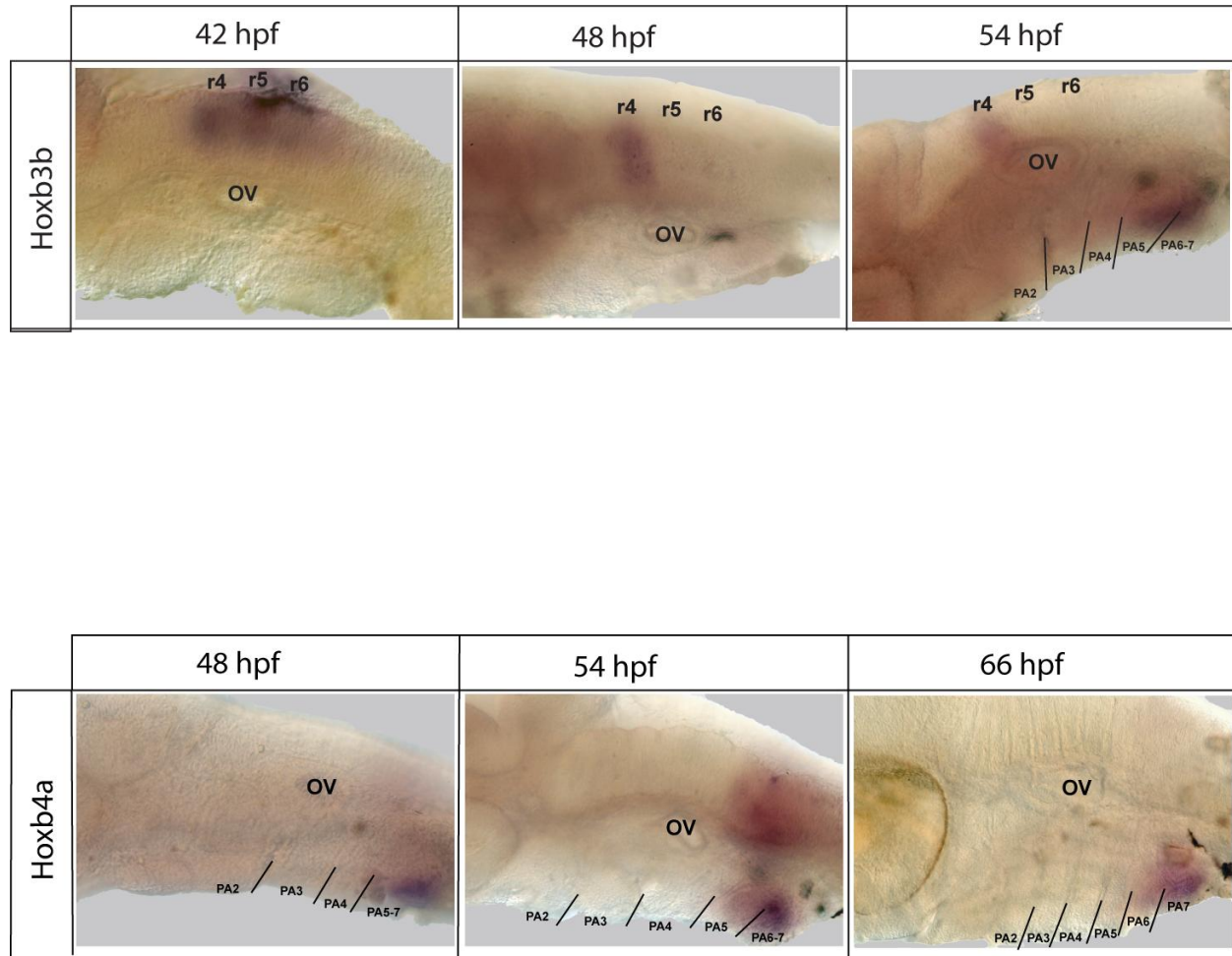


Fig 2. Pharyngeal expression of *hoxb3b* and *hoxb4a* genes in Nile tilapia embryos. All specimens are shown with dorsal to the top, anterior to the left. TOP-*hoxb3b* expression at 42 hpf, 48, hpf, and 54 hpf, from left to right. Expression is observed in rhombomeres 4-7 at 42 hpf. Expression observed in rhombomere 4 and pharyngeal arches (PA) 5-6 at 54 hpf. BOTTOM-*hoxb4a* expression at 48 hpf, 54 hpf, and 66 hpf, from left to right. Expression is observed within rhombomere 7, neural tube, and PA 5 at 48 hpf. Expression in PA 5-6 at 54 hpf. Expression in PA 6-7 exclusively by 66 hpf.

Figure 3: Lateral Views of Whole Mount *In Situ* Hybridization: Antisense Probes of *Hox* Paralogous Groups 5

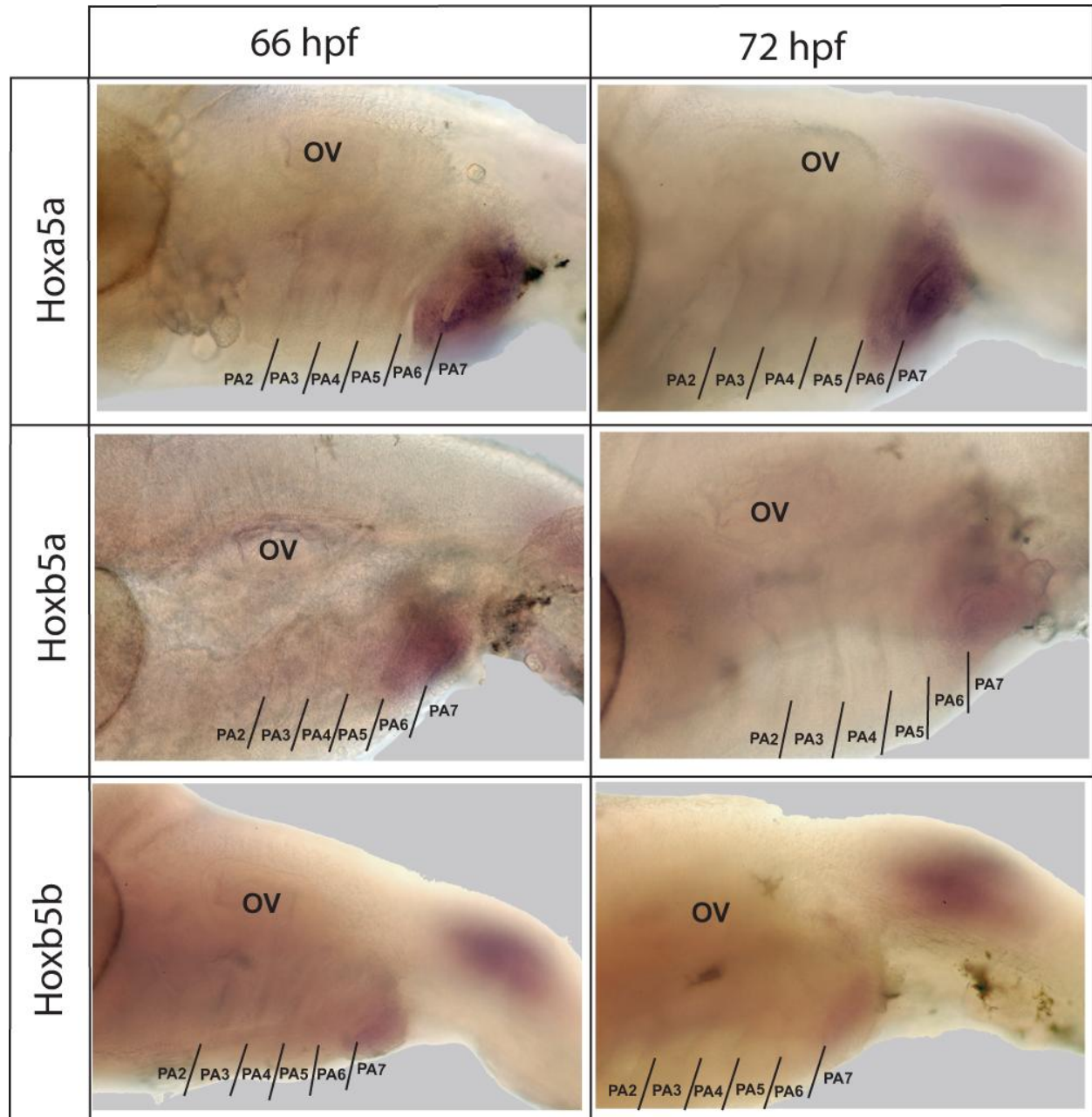


Fig 3. Pharyngeal expression of *hox* genes a5a, b5a, and b5b in Nile tilapia embryos at 66 hpf and 72 hpf (left to right). All specimens are shown with dorsal to the top, anterior to the left. *Hoxa5a* expression observed within PA 6-7 from 66-72, with neural tube expression at 72 hpf. *Hoxb5a* expression observed within PA 6-7 at 66 hpf. Expression observed in PA 7 at 72 hpf. *Hoxb5b* expression observed in PA 7 and anterior neural tube from 66-72 hpf.

Figure 4: Lateral Views of Whole Mount *In Situ* Hybridization: Antisense Probes of *Hox* Paralogous Group 6

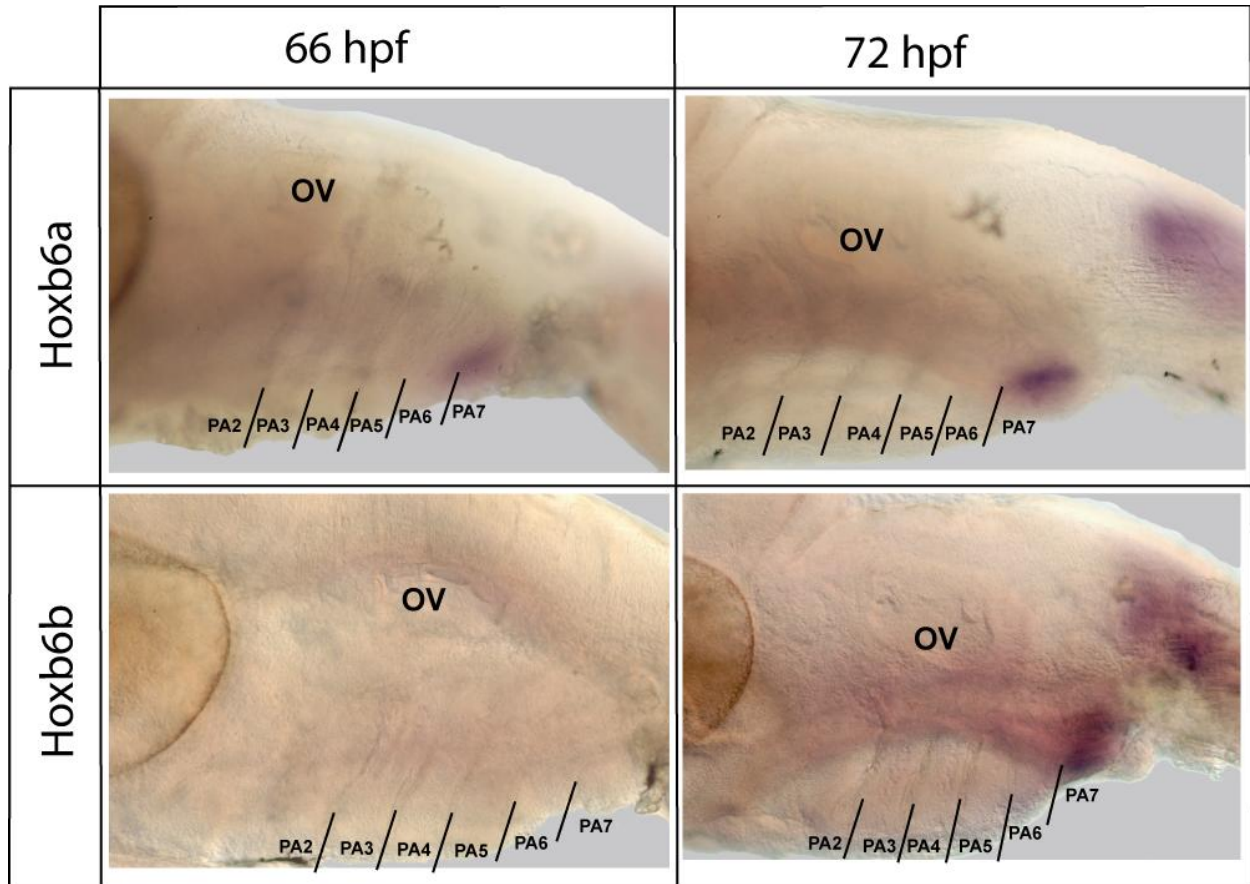


Fig 4. Pharyngeal expression of *hoxb6a* and *hoxb6b* genes in Nile tilapia embryos at 66 hpf and 72 hpf (left to right). All specimens are shown with dorsal to the top, anterior to the left. *Hoxb6a* expression is observed in PA 7 at 66 hpf; expression is within PA 7 and neural tube by 72 hpf. *Hoxb6b* expression is not observed at 66 hpf; expression is observed in PA 7 and the anterior neural tube at 72 hpf.

Figure 5: Combinatorial Code of *Hox* Expression in Nile tilapia Posterior Pharyngeal Arches

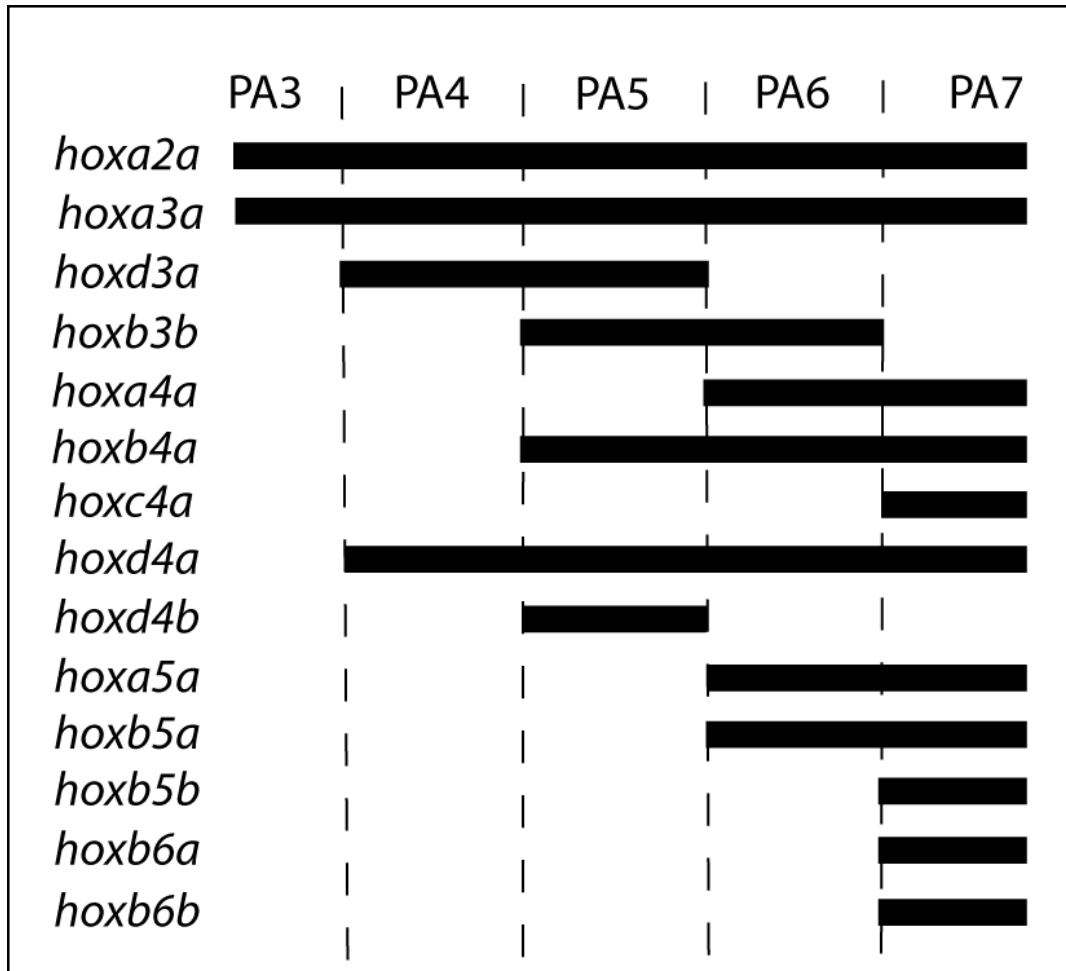


Fig 5. Combinatorial code of *hox* expression in Nile tilapia posterior pharyngeal arches. Modified from Le Pabic, 2009.

CHAPTER 4: DISCUSSION

Hox genes have been identified as essential developmental control genes, primarily responsible for patterning the anterior-posterior axis (Burke et al. 1995; Gilbert 2000; Wellik 2007). The combinatorial *hox* gene expression within a developing compartment, or *hox* code, has been shown to be paramount in determining the identity of the structure derived from that compartment (Hunt et al. 1991; Wellik 2007). Because *hox* genes are highly evolutionarily conserved in sequence and function, *hox* codes are thought to be a fundamental developmental mechanism common to invertebrate and vertebrate species and as such, any variation in a *hox* code could ultimately result in morphological variation (Gaunt 1994; Wagner et al. 2003).

While *hox* genes are known to be expressed in most tissues; the focus of the present study is *hox* gene expression within the pharyngeal arches. In developing vertebrates, the pharyngeal arches are a highly compartmentalized series of structures, each giving rise to specific skeletal and cartilaginous derivatives (Le Lievre et al. 1975; Piotrowski et al. 1996; Schilling et al. 1996; Le Pabic et al. 2009). The specific derivatives of each arch vary across species. Because of the morphological diversity found among the pharyngeal arch derived structures, it is inferred that each pharyngeal arch must have a unique molecular identity, allowing for proper specification of the arch derived structures. Misexpression studies of select *hox* genes have resulted in transformation of pharyngeal arch identity, as determined by homeotic transformation of pharyngeal arch derived structures (Gendron-Maguire et al. 1993; Rijli et al. 1993; Hunter et al. 2002; Baltzinger et al. 2005). Dr. Le Pabic's loss of function study of the *hoxa2a*, *hoxa2b*, and *hoxb2a* genes of *O. niloticus* embryos produced phenotypes consisting of the transformation of second pharyngeal arch derived cartilages into morphologies consistent with those derived from

the first pharyngeal arch. These findings intimately correlate *hox* gene expression to pharyngeal arch identity.

This investigation characterized *hox* expression within the developing pharyngeal arches of *Oreochromis niloticus* embryos via whole mount *in situ* hybridization. The data gathered indicates that each pharyngeal arch expresses a unique combination of *hox* genes. We have dubbed this pattern of expression the pharyngeal *hox* code. Although some pharyngeal *hox* expression data is available in other species, no previous study has been performed to fully characterize a pharyngeal *hox* code (Trainor et al. 2001; Hunter et al. 2002). Our findings extend the role of the vertebrate *hox* code to a novel compartment, the pharyngeal arches, and provide insight into the development of pharyngeal arch derived structures.

The *Oreochromis niloticus* *hox* expression data gathered in this investigation complements the *hox* expression data generated previously in our laboratory (Le Pabic et al. 2009). Furthermore, we have shown that there are intriguing similarities and differences among the pharyngeal *hox* expression in *Oreochromis niloticus* and other species. Comparison of the pharyngeal *hox* expression across multiple species would provide insight into any potential *hox* role in the evolutionary divergence of pharyngeal arch derived structure morphology across the species.

The *hox* paralogous group 3 genes investigated in this study were *hoxb3b* and *hoxc3a*. Transcripts for *hoxc3a* were not detected via *in situ* hybridization at any time point investigated. Multiple antisense riboprobes were designed in an attempt to gather expression data for *hoxc3a*, although all attempts were unsuccessful. We were successful, however, in amplifying partial cDNA for *hoxc3a* via RT-PCR. Our RT-PCR results indicate that *hoxc3a* expression peaks near 50 hpf. We believe that the discrepancy in the results of the two techniques is a consequence of

the sensitivity of the techniques. It is possible that a higher number of mRNA is necessary for analysis by *in situ* hybridization than it is for RT-PCR. Because cDNA used for RT-PCR was generated from a total RNA extraction, it is feasible that the total number of *hoxc3a* transcripts present in the embryo is high enough for detection via RT-PCR. Another possible explanation for the discrepancy is that the *hoxc3a* mRNA is found throughout the embryo, rather than concentrated into a compartmentalized tissue. The relatively low concentration of *hoxc3a* in any given tissue could thus be below the detectable limit via *in situ* hybridization. The original *hoxc3a* riboprobe developed is 389 bp in length. Of the 389 bp, 20.05%, or 78 nucleotides, are uracil nucleotides. Interestingly, this riboprobe for *hoxc3a* is unique for two reasons: it is the shortest of all the riboprobes developed in this study, and has the lowest specific activity as measured by incorporated digoxigenin labeled nucleotides. It is therefore possible that the lack of expression data generated from *in situ* hybridizations for *hoxc3a* is an effect of the combination of a riboprobe with low specific activity, and a potentially low mRNA concentration. *In situ* hybridizations were successful in generating expression data for all other *hox* genes investigated.

Hoxb3b was the remaining paralogous group 3 *hox* gene investigated in this study. The pharyngeal expression of *hoxb3b*, confined to pharyngeal arches 5 and 6, is unique to the localization of the two other paralogous group 3 genes investigated previously in our laboratory. Dr. Le Pabic discovered that *hoxa3a* was expressed in all posterior pharyngeal arches (3-7), and that *hoxd3a* was confined to pharyngeal arches 4 and 5 (Le Pabic et al. 2009). Curiously, *hox A3* has been reported to be necessary for the proper morphological development and timing of development of pharyngeal arch 3 in the mouse (Chisaka et al. 2005). Murine *hox A3* has been shown to be required for the development and migration of the thymus, the thyroid, and the

parathyroid glands-all of which are derived from the third and fourth pharyngeal arches (Manley et al. 1998). The same study indicated that although expressed, murine *hox B3* and *hox D3* do not share this function, and when knocked out, produce no visible morphological phenotype. Further murine experimentation has revealed that *hox A2* and *hox A3* act synergistically to pattern both the third and fourth pharyngeal arches (Minoux et al. 2009). As previously stated, it has been shown that of the *Oreochromis niloticus* paralogous group 3 genes, only *hoxa3a* is expressed within the third pharyngeal arch. It is thus possible to speculate that *hoxa3a* performs a necessary role in the patterning of the third pharyngeal arch in *Oreochromis niloticus*. Because *hoxa3a* is present in all posterior pharyngeal arches of *Oreochromis niloticus* while *hoxb3b* and *hoxd3a* both have distinct anterior pharyngeal expression limits, the question of molecular significance of all three of the paralogous genes is raised. No experimentation has been performed which examines the specific roles of the *Oreochromis niloticus* *hoxb3b* or *hoxd3a* genes in patterning the posterior pharyngeal arches, and thus it is unknown whether these *hox* genes have molecular functions that are independent of or redundant to that of *hoxa3a*.

Hoxb4a was the only member of *hox* paralogous group 4 to be investigated by this study, as most members of this paralogous group were investigated previously by Dr. Le Pabic. He identified *hoxa4a*, *hoxc4a*, *hoxd4a*, and *hoxd4b* as the genes expressed within the posterior pharyngeal arches, however their expression patterns are quite diverse (Le Pabic et al. 2009). *Hoxa4a* is localized to pharyngeal arches 6 and 7. *Hoxc4a* is only found within pharyngeal arch 7. *Hox D4a* presents the most ubiquitous pharyngeal expression pattern, with expression found in pharyngeal arches 4-7. Finally, *hoxd4b* was exclusively localized to pharyngeal arch 5. *Hoxb4a*, characterized in this study, was found to be expressed within pharyngeal arches 5-7, although expression within pharyngeal arch 5 was transient and was undetectable by 72 hpf.

Unfortunately very little is known concerning *hox* paralogous group 4 gene expressions in other species, especially the common experimental organisms mouse and zebrafish. Studies in flounder development, however, have indicated that that *hox* D4 is expressed in pharyngeal arches 3-7 under natural conditions (Suzuki et al. 1999). When treated with retinoic acid, however, the flounder *hox* D4 anterior expression limit is shifted in the anterior direction, implying a role for *hox* D4 in patterning the third pharyngeal arch of flounder (Suzuki et al. 1999). Unlike in flounder, no Nile tilapia *hox* paralogous group 4 genes are expressed anterior of pharyngeal arch 4. As stated, no data concerning the zebrafish pharyngeal expression of *hox* paralogous group 4 is known. Curiously, however, *hoxd4b* has been lost in the zebrafish lineage (Le Pabic et al. 2009). Its presence in the Nile tilapia *hox* gene complement, and its distinct expression in the fifth pharyngeal arch indicates that *hoxd4b* could be an important selector gene for the identity of pharyngeal arch 5 in Nile tilapia (Le Pabic et al. 2009). *Hoxb4a* is the only other paralogous group 4 gene with an anterior pharyngeal expression limit of pharyngeal arch 5, therefore any investigation concerning the pharyngeal role of *hoxd4b* in Nile tilapia would also require exploration of the *hoxb4a* gene, as the two may have overlapping molecular functions.

Three of the eight *Oreochromis niloticus* *hox* genes localized in this study belong to the *hox* paralogous group 5. *Hoxc5a* is the only paralogous group 5 gene to have been previously examined by Dr. Le Pabic, and its expression was shown to be confined to the neural tube, with no pharyngeal expression (Le Pabic et al. 2009). *Hoxa5a* was shown to be robustly expressed within pharyngeal arches 6-7, from 66 hpf through 72 hpf. *Hoxb5a* was also shown to be expressed within pharyngeal arches 6-7 from 66 hpf through 72 hpf, although by 72 hpf the expression appears weaker. The transient pattern of expression observed for *hoxb5a*, as opposed to the persistent and robust expression of *hoxa5a*, could potentially indicate that the pharyngeal

molecular function of *hoxb5a* is more important to patterning pharyngeal arch 6 than pharyngeal arch 7. It is also possible that *hoxb5a* could have a redundant role to *hoxa5a*, or vice versa.

Intriguingly, pharyngeal arch 7 was the only pharyngeal arch to express *hoxb5b* transcripts. In similar fashion to *hoxb5a* transcripts, *hoxb5b* transcripts appeared to peak in expression at 66 hpf and began to diminish by 72 hpf. It is important to note that the combined expression patterns of *hoxb5a* and *hoxb5b* mirror the expression of *hoxa5a* at 66 hpf. Studies in zebrafish have indicated that *hoxb5a* and *hoxb5b* expression localizations are distinct, yet together mirror the expression of the *hoxB5* gene in chicken, frog, and mouse (Bruce et al. 2001). The authors of the study suggest that the zebrafish *hoxb5a* and *hoxb5b* genes have evolutionarily subfunctionalized as a result of the teleostean genome duplication event. An important contrast with Nile tilapia, however, is the precise location of expression of the zebrafish and mouse *hox B5* orthologs. In zebrafish, *hoxb5a* is expressed within the posterior pharyngeal arches, while *hoxb5b* is not (Bruce et al. 2001). In mouse, *hox B5* is expressed within the posterior pharyngeal arches (Jarínova et al. 2008). In both zebrafish and mouse, all previously mentioned *hoxB5* orthologs are expressed in the posterior hindbrain and neural tube (Bruce et al. 2001; Jarínova et al. 2008). Our investigation has revealed that in Nile tilapia, in addition to posterior arch expression, *hoxb5a* and *hoxb5b* are expressed within the neural tube. No expression, however, was observed in the posterior hindbrain of developing Nile tilapia embryos. An interesting addition to the multispecies comparison of *hoxB5* ortholog expression patterns is that of the flounder. It is known that the flounder *hox B5* gene is expressed within pharyngeal arch 7 and the neural tube (Suzuki et al. 1999). Clearly there is conservation in expression patterns of *hox B5* orthologs across many species, implying a conserved function in patterning the most posterior pharyngeal arches and neural tube. Unfortunately the bulk of research that has been performed on *hox*

paralogous group 5 genes have been focused on the *hox* B5 orthologs. A multispecies analysis concerning the *hox* A5 orthologs would be of great relevance to our investigation, as *hox* A5a in Nile tilapia appears to be one the most robustly expressed *hox* genes we have investigated. Nile tilapia misexpression studies of the *hox* paralogous group 5 genes would add tremendous insight into the possible subfunctionalization of the teleost *hoxb5a* and *hoxb5b* genes. The independent molecular roles of Nile tilapia *hoxa5a*, *hoxb5a*, and *hoxb5b* genes should be examined.

Hox paralogous group 6 genes were also investigated in our study. The Nile tilapia *hoxb6a* and *hoxb6b* genes were investigated in this study, and *hoxc6a* was previously investigated in our laboratory by Dr. Le Pabic. Both *hoxb6a* and *hoxb6b* were shown to be expressed within pharyngeal arch 7 and the neural tube, posterior of the pharyngeal arches. The onset of expression of *hoxb6b* was delayed compared to that of *hoxb6a*, however both genes are clearly expressed by 72 hpf. Interestingly, Dr. Le Pabic's study revealed that *hoxc6a* was strictly confined to the neural tube. We are not aware of any previous studies revealing *hox* paralogous group 6 gene expression within the pharyngeal arches. Studies of the chick and quail reveal that *hox* A6 and *hox* C6 are expressed within the somites, although *hox* B6 is not addressed (Nowicki et al. 2000). Further investigations using teleost species are required in order to ascertain whether or not pharyngeal expression of the *hox* paralogous group 6 genes is specific to Nile tilapia. Murine studies would also be significant, potentially revealing a correlation between diverse *hox* paralogous group 6 gene expression and the diverse morphologies that exist among fish, avian, and mammalian species.

It is important to note that although our study has found *hox* gene expression within the pharyngeal arches and neural tube of Nile tilapia embryos, no somitic expression was observed. This is certainly in direct contrast to work performed in other vertebrate species, including the

chick and mouse (Kessel et al. 1990; Burke et al. 1995). As previously discussed, the *hox* code is very well known for patterning the anterior-posterior axis along developing somites in vertebrate species. In mice, *hox* paralogous groups 4-6 are expressed within somites that give rise to the cervical and anterior thoracic vertebrae (Wellik 2007). It is curious that no members of these paralogous groups were shown to be expressed within the somites of developing Nile tilapia embryos. It is possible that somitic expression of these *hox* genes in Nile tilapia embryos is present, and is simply indiscernible. Somites are not readily visible in Nile tilapia embryos until approximately 66 hpf. Section *in situ* hybridizations would need to be performed in order to conclusively elucidate somitic expression of *hox* genes within developing Nile tilapia embryos.

A striking conclusion that can be drawn from the summation (Figure 5) of our laboratory's findings is that *hox* gene expression within the pharyngeal arches appears to largely exhibit colinearity. The phenomenon of colinearity has long been established among researchers of *hox* genes. The organization of *hox* genes on the chromosomes often parallels the temporal and spatial expression patterns of the *hox* genes themselves (Krumlauf 1994; Duboule 1998). *Hox* genes from lower paralogous groups have been shown to be expressed in more anterior locations in a developing embryo than *hox* genes from higher paralogous groups. In addition, *hox* genes from the lower paralogous groups typically will begin to be expressed at earlier developmental time points than those *hox* genes from higher paralogous groups. As previously stated, our findings support this unique characteristic of *hox* gene expression. Referring to Figure 5, it is seen that with few exceptions, *hox* genes from lower paralogous groups have more anterior limits to pharyngeal arch expression, while *hox* genes from higher paralogous groups have anterior pharyngeal expression limits that are shifted in a more posterior direction.

As previously discussed, our investigation is the first to comprehensively explore the expression of *hox* genes within the pharyngeal arches of a developing organism. Pharyngeal arch 3 has been shown to express *hoxa2a* and *hoxa3a*. The *hox* expression within pharyngeal arch 4 is similar to that of pharyngeal arch 3, with the addition of two *hox* genes: *d3a* and *d4a*. Pharyngeal arch 5 continues to express the *hox* genes found within pharyngeal arches 3 and 4, as well as *hox* genes *b3b*, *b4a*, and *d4b*. *Hox* expression within pharyngeal arch 6 is more diverse than the previous arches. In pharyngeal arch 6, all the *hox* genes expressed in pharyngeal arch 5 are present, with the following notable exceptions: *hox* genes *D3a* and *D4b* are excluded, and *hox* genes *a4a*, *a5a*, and *b5a* are included. Lastly, pharyngeal arch 7 is host to numerous expressed *hox* genes. Of all the pharyngeal arches, pharyngeal arch 7 expresses the highest number of *hox* genes. The expression in pharyngeal arch 7 is similar to that of pharyngeal arch 6, having lost only *hoxb3b*. Four *hox* genes, *hoxc4a*, *b5b*, *b6a*, and *b6b*, have anterior pharyngeal expression limits that begin in pharyngeal arch 7. Our results clearly demonstrate that within each pharyngeal arch is expressed a unique combination of *hox* genes, or pharyngeal *hox* code (Figure 5).

Of notable interest, we have shown that *hox* genes expressed within the pharyngeal arches have distinct anterior expression limits. Often the expression of the *hox* genes extends in the posterior direction, spanning several pharyngeal arches and persisting throughout the later time points investigated here. The sharp anterior limit of expression has been shown to be important in establishing the role for *hox* genes in a particular tissue, and has been coined by Dr. Denis Duboule as the *hox* posterior prevalence theory (Duboule 1991; Lufkin et al. 1991; Duboule et al. 1994). Some research has suggested that the *hox* complement expressed within or near a developing pharyngeal arch can in turn regulate the expression of other *hox* genes. A

study utilizing zebrafish has shown that the ectopic expression of either *hoxb5a* or *hoxb5b* results in the decreased expression of both *hoxa2b* and *hoxb2a*, specifically within neural crest cells of the hyoid neural crest stream, ultimately bound for pharyngeal arch 2 (Bruce et al. 2001).

Morphological transformations then occurred, resulting in a loss of specific structures derived from pharyngeal arch 2. In this situation, the usually more posterior paralogous group 5 *hox* genes assume prevalence in the molecular patterning of the pharyngeal arches. After reviewing the Nile tilapia expression data gathered from our study, it is reasonable to speculate that similar misexpression studies with the Nile tilapia would provide similar results. Perhaps there is no better starting point for such an investigation than within pharyngeal arch 7. As previously discussed, pharyngeal arch 7 of Nile tilapia contains the highest number of expressed *hox* genes of any of the pharyngeal arches. Four of the *hox* genes investigated are localized exclusively to pharyngeal arch 7, in addition to the numerous other *hox* genes also expressed in more anterior pharyngeal arches. The ectopic expression of any of the four *hox* genes expressed exclusively within pharyngeal arch 7 would likely result in the posteriorization of anterior pharyngeal arch derived cartilages.

Although all of the pharyngeal arches give rise to unique structures in the Nile tilapia, pharyngeal arch 7 is quite unique. Dr. Le Pabic's research with the Nile tilapia revealed that the posterior pharyngeal arches (arches 3-7) collectively derive the cartilaginous and skeletal components of the pharyngeal jaw apparatus, a secondary set of jaws unique to some perciform fishes (Le Pabic et al. 2009). Pharyngeal arch 7, however, is exclusively responsible for deriving the most posterior ceratobranchial cartilage, ceratobranchial 5, as well as the lower tooth plate (Le Pabic et al. 2009). Dr. Le Pabic speculated that the lower tooth plate was the most active component of the pharyngeal jaw apparatus with regard to food processing (Le Pabic et al.

2009). Considering the very specific and highly important derivatives of pharyngeal arch 7, it is easy to speculate that the unique combinatorial array of *hox* gene expression within pharyngeal arch 7 is required for the derivation of the previously mentioned structures.

The *hox* expression data generated from this investigation, in cooperation with previously discussed *hox* gene misexpression studies in the Nile tilapia, zebrafish, and mouse, strongly supports the pharyngeal *hox* code as being the molecular mechanism responsible for pharyngeal arch patterning. Future extensions of previous experimentation could unequivocally support the molecular role of the pharyngeal *hox* code. For example, Dr. Le Pabic's knockdown experiments of *hox* paralogous group 2 genes could be repeated, or extended to include *hox* genes of other paralogous groups. *In situ* hybridizations could then be performed on the embryos to determine if the misexpression of *hox* genes caused unexpected changes in the composition of the pharyngeal *hox* code. Any homeotic transformations observed in pharyngeal arch derived cartilages could then potentially be directly linked to definite transformations of the pharyngeal *hox* code.

The *hox* genes, although extensively studied, continue to be revealed as fundamental pleiotropic developmental genes. Here we have presented a novel *hox* code-the pharyngeal *hox* code. Based on our findings, we extend the prediction that the unique combination of *hox* genes shown to be expressed in each pharyngeal arch is responsible for establishing molecular pharyngeal arch identity, and thus the identities and resulting morphologies of all pharyngeal arch derived structures.

REFERENCES

- Amores, A., A. Force, et al. (1998). "Zebrafish hox clusters and vertebrate genome evolution." Science **282**(5394): 1711-4.
- Baltzinger, M., M. Ori, et al. (2005). "Hoxa2 knockdown in *Xenopus* results in hyoid to mandibular homeosis." Dev Dyn **234**(4): 858-67.
- Bruce, A. E., A. C. Oates, et al. (2001). "Additional hox clusters in the zebrafish: divergent expression patterns belie equivalent activities of duplicate hoxB5 genes." Evol Dev **3**(3): 127-44.
- Burke, A. C., C. E. Nelson, et al. (1995). "Hox genes and the evolution of vertebrate axial morphology." Development **121**(2): 333-46.
- Capovilla, M. and J. Botas (1998). "Functional dominance among Hox genes: repression dominates activation in the regulation of Dpp." Development **125**(24): 4949-57.
- Chisaka, O. and Y. Kameda (2005). "Hoxa3 regulates the proliferation and differentiation of the third pharyngeal arch mesenchyme in mice." Cell Tissue Res **320**(1): 77-89.
- Chiu, C. H., D. Nonaka, et al. (2000). "Evolution of Hoxa-11 in lineages phylogenetically positioned along the fin-limb transition." Mol Phylogenet Evol **17**(2): 305-16.
- Choe, S. K., N. Vlachakis, et al. (2002). "Meis family proteins are required for hindbrain development in the zebrafish." Development **129**(3): 585-95.
- Duboule, D. (1991). "Patterning in the vertebrate limb." Curr Opin Genet Dev **1**(2): 211-6.
- Duboule, D. (1998). "Vertebrate hox gene regulation: clustering and/or colinearity?" Curr Opin Genet Dev **8**(5): 514-8.
- Duboule, D. and G. Morata (1994). "Colinearity and functional hierarchy among genes of the homeotic complexes." Trends Genet **10**(10): 358-64.
- Fujimura, K. and N. Okada (2007). "Development of the embryo, larva and early juvenile of Nile tilapia *Oreochromis niloticus* (Pisces: Cichlidae). Developmental staging system." Dev Growth Differ **49**(4): 301-24.
- Furlong, R. F. and P. W. H. Holland (2004). "Polyploidy in vertebrate ancestry: Ohno and beyond." Biological Journal of the Linnean Society **82**(4): 425-430.
- Gaunt, S. J. (1994). "Conservation in the Hox code during morphological evolution." Int J Dev Biol **38**(3): 549-52.

- Gendron-Maguire, M., M. Mallo, et al. (1993). "Hoxa-2 mutant mice exhibit homeotic transformation of skeletal elements derived from cranial neural crest." Cell **75**(7): 1317-31.
- Gilbert, S. F. (2000). Developmental biology. Sunderland, Mass., Sinauer Associates.
- Grammatopoulos, G. A., E. Bell, et al. (2000). "Homeotic transformation of branchial arch identity after Hoxa2 overexpression." Development **127**(24): 5355-65.
- Hoegg, S., J. L. Boore, et al. (2007). "Comparative phylogenomic analyses of teleost fish Hox gene clusters: lessons from the cichlid fish *Astatotilapia burtoni*." BMC Genomics **8**: 317.
- Hughes, A. L. (1999). "Phylogenies of developmentally important proteins do not support the hypothesis of two rounds of genome duplication early in vertebrate history." J Mol Evol **48**(5): 565-76.
- Hunt, P. and R. Krumlauf (1991). "Deciphering the Hox code: clues to patterning branchial regions of the head." Cell **66**(6): 1075-8.
- Hunter, M. P. and V. E. Prince (2002). "Zebrafish hox paralogue group 2 genes function redundantly as selector genes to pattern the second pharyngeal arch." Dev Biol **247**(2): 367-89.
- Hurley, I., M. E. Hale, et al. (2005). "Duplication events and the evolution of segmental identity." Evol Dev **7**(6): 556-67.
- Jaillon, O., J. M. Aury, et al. (2004). "Genome duplication in the teleost fish *Tetraodon nigroviridis* reveals the early vertebrate proto-karyotype." Nature **431**(7011): 946-57.
- Jarinova, O., G. Hatch, et al. (2008). "Functional resolution of duplicated hoxb5 genes in teleosts." Development **135**(21): 3543-53.
- Kessel, M. and P. Gruss (1990). "Murine developmental control genes." Science **249**(4967): 374-9.
- Knoepfler, P. S., Q. Lu, et al. (1996). "Pbx-1 Hox heterodimers bind DNA on inseparable half-sites that permit intrinsic DNA binding specificity of the Hox partner at nucleotides 3' to a TAAT motif." Nucleic Acids Res **24**(12): 2288-94.
- Krumlauf, R. (1992). "Evolution of the vertebrate Hox homeobox genes." Bioessays **14**(4): 245-52.
- Krumlauf, R. (1994). "Hox genes in vertebrate development." Cell **78**(2): 191-201.
- Le Lievre, C. S. and N. M. Le Douarin (1975). "Mesenchymal derivatives of the neural crest: analysis of chimaeric quail and chick embryos." J Embryol Exp Morphol **34**(1): 125-54.
- Le Pabic, P., E. J. Stellwag, et al. (2007). "Comparative analysis of Hox paralog group 2 gene expression during Nile tilapia (*Oreochromis niloticus*) embryonic development." Dev Genes Evol **217**(11-12): 749-58.

- Le Pabic, P., E. J. Stellwag, et al. (2009). "Embryonic Development and Skeletogenesis of the Pharyngeal Jaw Apparatus in the Cichlid Nile Tilapia (*Oreochromis niloticus*)."
Anat Rec (Hoboken).
- Lewis, E. B. (1978). "A gene complex controlling segmentation in *Drosophila*." Nature **276**(5688): 565-70.
- Lohmann, I. (2003). "Dissecting the regulation of the *Drosophila* cell death activator reaper." Gene Expr Patterns **3**(2): 159-63.
- Lohmann, I., N. McGinnis, et al. (2002). "The *Drosophila* Hox gene *deformed* sculpts head morphology via direct regulation of the apoptosis activator reaper." Cell **110**(4): 457-66.
- Lufkin, T., A. Dierich, et al. (1991). "Disruption of the Hox-1.6 homeobox gene results in defects in a region corresponding to its rostral domain of expression." Cell **66**(6): 1105-19.
- Manley, N. R. and M. R. Capecchi (1998). "Hox group 3 paralogs regulate the development and migration of the thymus, thyroid, and parathyroid glands." Dev Biol **195**(1): 1-15.
- Mann, R. S., K. M. Lelli, et al. (2009). "Hox specificity unique roles for cofactors and collaborators." Curr Top Dev Biol **88**: 63-101.
- Mastick, G. S., R. McKay, et al. (1995). "Identification of target genes regulated by homeotic proteins in *Drosophila melanogaster* through genetic selection of Ultrabithorax protein-binding sites in yeast." Genetics **139**(1): 349-63.
- Minoux, M., G. S. Antonarakis, et al. (2009). "Rostral and caudal pharyngeal arches share a common neural crest ground pattern." Development **136**(4): 637-45.
- Nowicki, J. L. and A. C. Burke (2000). "Hox genes and morphological identity: axial versus lateral patterning in the vertebrate mesoderm." Development **127**(19): 4265-75.
- Ohno, S. (1970). Evolution by gene duplication. London, New York, Allen & Unwin; Springer-Verlag.
- Pasqualetti, M., M. Ori, et al. (2000). "Ectopic Hoxa2 induction after neural crest migration results in homeosis of jaw elements in *Xenopus*." Development **127**(24): 5367-78.
- Patel, N. H. and V. E. Prince (2000). "Beyond the Hox complex." Genome Biol **1**(5): REVIEWS1027.
- Piotrowski, T., T. F. Schilling, et al. (1996). "Jaw and branchial arch mutants in zebrafish II: anterior arches and cartilage differentiation." Development **123**: 345-56.
- Rijli, F. M., M. Mark, et al. (1993). "A homeotic transformation is generated in the rostral branchial region of the head by disruption of Hoxa-2, which acts as a selector gene." Cell **75**(7): 1333-49.

- Santini, S. and G. Bernardi (2005). "Organization and base composition of tilapia Hox genes: implications for the evolution of Hox clusters in fish." Gene **346**: 51-61.
- Schilling, T. F. and C. B. Kimmel (1994). "Segment and cell type lineage restrictions during pharyngeal arch development in the zebrafish embryo." Development **120**(3): 483-94.
- Schilling, T. F., T. Piotrowski, et al. (1996). "Jaw and branchial arch mutants in zebrafish I: branchial arches." Development **123**: 329-44.
- Scott, M. P. (1993). "A rational nomenclature for vertebrate homeobox (HOX) genes." Nucleic Acids Res **21**(8): 1687-8.
- Suzuki, T., I. Oohara, et al. (1999). "Retinoic acid given at late embryonic stage depresses sonic hedgehog and Hoxd-4 expression in the pharyngeal area and induces skeletal malformation in flounder (*Paralichthys olivaceus*) embryos." Dev Growth Differ **41**(2): 143-52.
- Suzuki, T., A. S. Srivastava, et al. (1999). "Hoxb-5 is expressed in gill arch 5 during pharyngeal arch development of flounder *Paralichthys olivaceus* embryos." Int J Dev Biol **43**(4): 357-9.
- Taylor, J. S., I. Braasch, et al. (2003). "Genome duplication, a trait shared by 22000 species of ray-finned fish." Genome Res **13**(3): 382-90.
- Trainor, P. A. and R. Krumlauf (2000). "Patterning the cranial neural crest: hindbrain segmentation and Hox gene plasticity." Nat Rev Neurosci **1**(2): 116-24.
- Trainor, P. A. and R. Krumlauf (2001). "Hox genes, neural crest cells and branchial arch patterning." Curr Opin Cell Biol **13**(6): 698-705.
- Vachon, G., B. Cohen, et al. (1992). "Homeotic genes of the Bithorax complex repress limb development in the abdomen of the *Drosophila* embryo through the target gene *Distal-less*." Cell **71**(3): 437-50.
- Van de Peer, Y., J. S. Taylor, et al. (2001). "The ghost of selection past: rates of evolution and functional divergence of anciently duplicated genes." J Mol Evol **53**(4-5): 436-46.
- Wagner, G. P., C. Amemiya, et al. (2003). "Hox cluster duplications and the opportunity for evolutionary novelties." Proc Natl Acad Sci U S A **100**(25): 14603-6.
- Wellik, D. M. (2007). "Hox patterning of the vertebrate axial skeleton." Dev Dyn **236**(9): 2454-63.
- Wellik, D. M. and M. R. Capecchi (2003). "Hox10 and Hox11 genes are required to globally pattern the mammalian skeleton." Science **301**(5631): 363-7.

APPENDIX A:
Supporting Information for Materials and Methods

Table 1: Sequence Accession Information

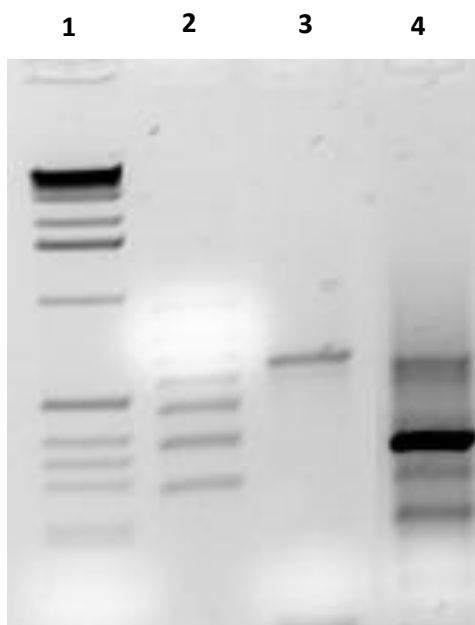
Species	<i>Hox</i> Gene Name	NCBI Accession Number
<i>O. niloticus</i>	b3b	AY757333
<i>O. niloticus</i>	c3a	AY757336
<i>O. niloticus</i>	b4a	AY757325
<i>O. niloticus</i>	b5a	AY757326
<i>O. niloticus</i>	b5b	AY757334
<i>O. niloticus</i>	b6a	AY757327
<i>O. niloticus</i>	b6b	AY757335
<i>A. burtoni</i>	b3b	EF594314
<i>A. burtoni</i>	c3a	EF594312
<i>A. burtoni</i>	a5a	EF594313
<i>A. burtoni</i>	b5a	EF594310
<i>A. burtoni</i>	b5b	EF594314
<i>A. burtoni</i>	b6a	EF594310
<i>A. burtoni</i>	b6b	EF594314

Table 2: PCR Information

PRIMER NAME	SEQUENCE (5' → 3')	OPTIMAL T _m (°C)	EXPECTED cDNA AMPLICON (bp)
b3b-F2	GCGCTTCACATAGCATCCATCA	61.5	677
b3b-R2	TGCGTGAAGCCTGAAACTGGAT	61.5	677
c3a-F2	CGGGATACAATGAAGGAGGAGGA	64.0	355
c3a-R2	TAGGACGACACAGGTAAGGGCTGA	64.0	355
b4a-F5	CAACTATGTGGACCCGAAGTT	61.0	610
b4a-R5	CATACGCCGGTTCTGAAACCA	61.0	610
a5a-F2	GACCACAGTACGGCAAACGAGCAA	61.9	526
a5a-R2	AGTGTATGCAGTTCTGGCCCGCTT	61.9	526
b5a-F2	GGATCAAGCAGGAAGCGGTAA	50.7	436
b5a-R2	TTTAATCTGCCGCTCCGTGA	50.7	436
b5b-F3	ACTAAAAAGCCCCTCTCCTCCCTC	64.6	341
b5b-R3	TACGCAGTTCGGGCCCTTTT	64.6	341
b6a-F3	CCACGAGTTTCTACAGGGAT	58.3	401
b6a-R3	CAGCTTGTTCTCCTTCTTCC	58.3	401
b6b-F3	CAGCCGCTGTTTGTCCTCA	64.6	389
b6b-R3	TTTCTCCGCTGTTCTCCTCT	64.6	389

Figure 1 (A-D): RT-PCR of selected *hox* genes used for molecular cloning. Images are the results of 1.5% gel electrophoresis of amplified cDNA. Lanes are numerically labeled on each image, with descriptions immediately below the images.

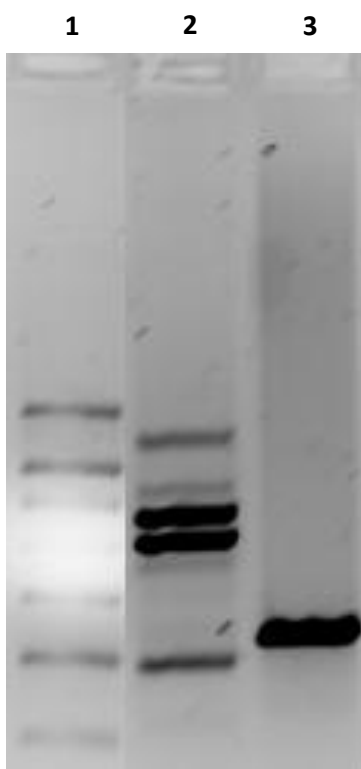
Fig. 1A



Lane Descriptions: (1) 1 Kb ladder, (2) 300-1000 bp ladder, (3) *hoxb3b* amplicon, (4) *hoxc3a* amplicon

Figure 1 (A-D): RT-PCR of selected *hox* genes used for molecular cloning. Images are the results of 1.5% gel electrophoresis of amplified cDNA. Lanes are numerically labeled on each image, with descriptions immediately below the images.

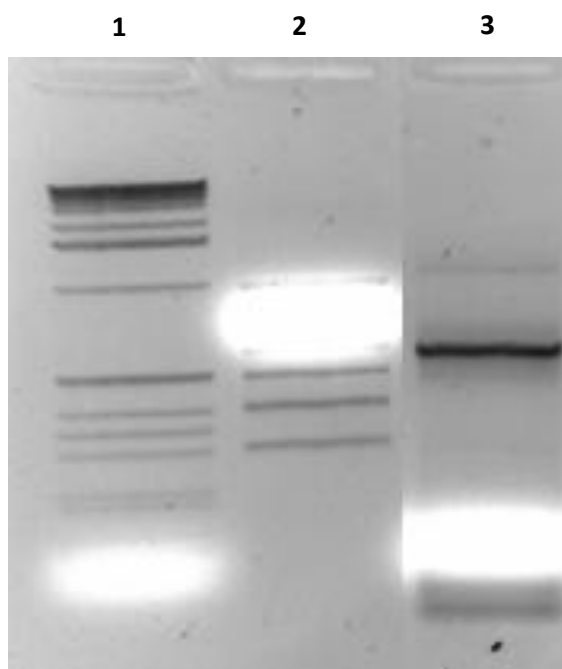
Fig. 1B



Lane Descriptions: (1) 300-1000 bp ladder, (2) *hoxb4a* amplicon, (3) *hoxb5a* amplicon

Figure 1 (A-D): RT-PCR of selected *hox* genes used for molecular cloning. Images are the results of 1.5% gel electrophoresis of amplified cDNA. Lanes are numerically labeled on each image, with descriptions immediately below the images.

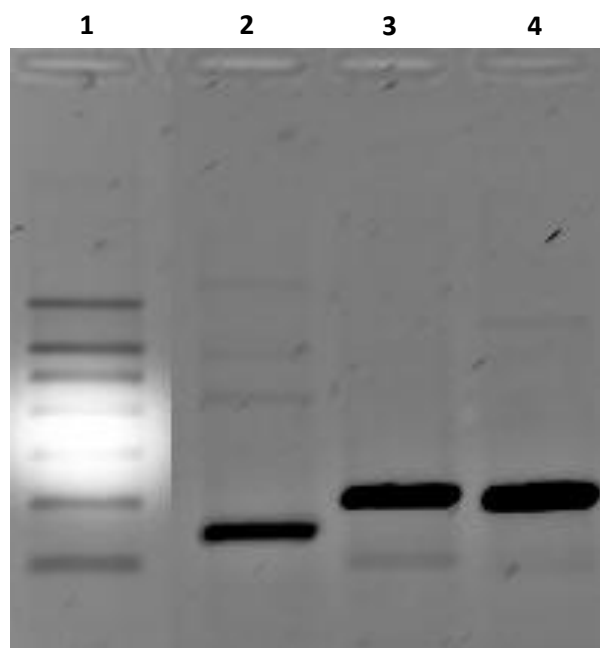
Fig. 1C



Lane Descriptions: (1) 1 Kb ladder, (2) 300-1000 bp ladder, (3) *hoxa5a* amplicon

Figure 1 (A-D): RT-PCR of selected *hox* genes used for molecular cloning. Images are the results of 1.5% gel electrophoresis of amplified cDNA. Lanes are numerically labeled on each image, with descriptions immediately below the images.

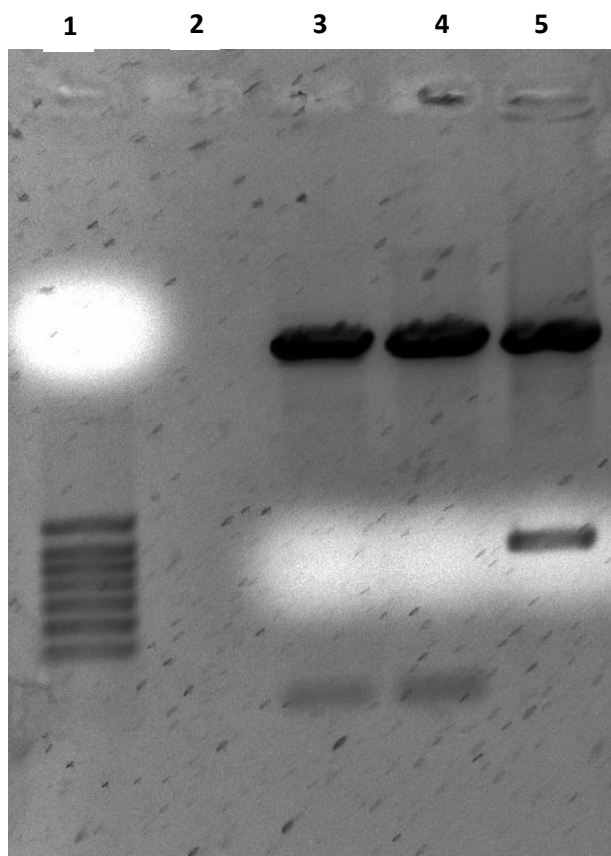
Fig. 1D



Lane Descriptions: (1) 300-1000 bp ladder, (2) *hoxb5b* amplicon, (3) *hoxb6a* amplicon, (4) *hoxb6b* amplicon

Figure 2 (A-D): Digested Plasmid Gel Electrophoresis Images. 1.5% gel electrophoresis was performed following EcoRI restriction enzyme digestions of purified plasmids. The electrophoresis was performed to screen recombinant plasmids for the appropriate inserts. Lanes are numerically labeled, and descriptions are found below each image.

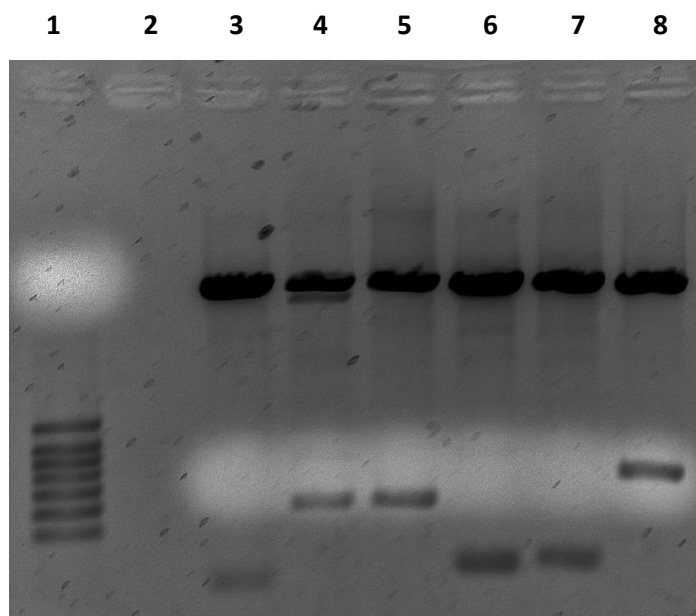
Fig 2A



Lane Descriptions: (1) 300-1000 bp ladder, (2) empty, (3) *hoxb3b* plasmid #1, (4) *hoxb3b* plasmid #2, (5) *hoxb3b* plasmid #3 with correct insert.

Figure 2 (A-D): Digested Plasmid Gel Electrophoresis Images. 1.5% gel electrophoresis was performed following EcoRI restriction enzyme digestions of purified plasmids. The electrophoresis was performed to screen recombinant plasmids for the appropriate inserts. Lanes are numerically labeled, and descriptions are found below each image.

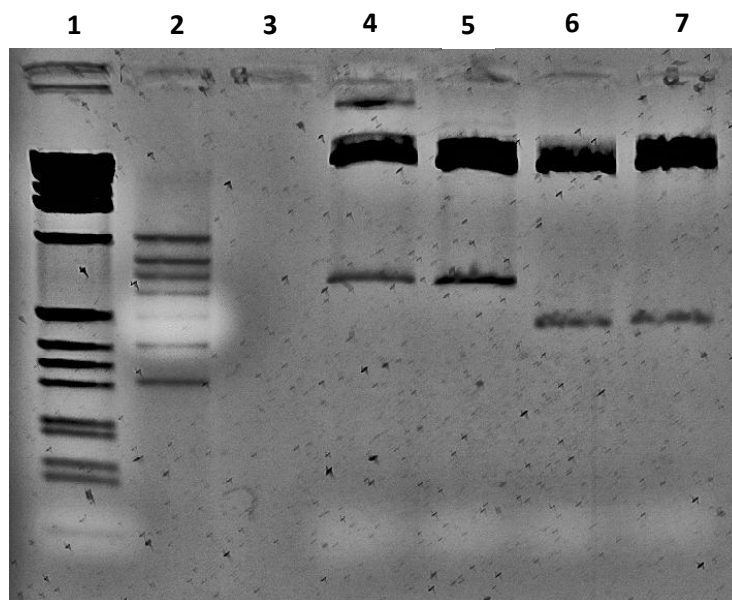
Fig 2B



Lane Descriptions: (1) 300-1000 bp ladder, (2) empty, (3) *hoxc3a* plasmid #1, (4) *hoxc3a* plasmid #2 containing correct insert, (5) *hoxc3a* plasmid #3 containing correct insert, (6) *hoxa5a* plasmid #1, (7) *hoxa5a* plasmid #2, (8) *hoxa5a* plasmid #3 containing correct insert.

Figure 2 (A-D): Digested Plasmid Gel Electrophoresis Images. 1.5% gel electrophoresis was performed following EcoRI restriction enzyme digestions of purified plasmids. The electrophoresis was performed to screen recombinant plasmids for the appropriate inserts. Lanes are numerically labeled, and descriptions are found below each image.

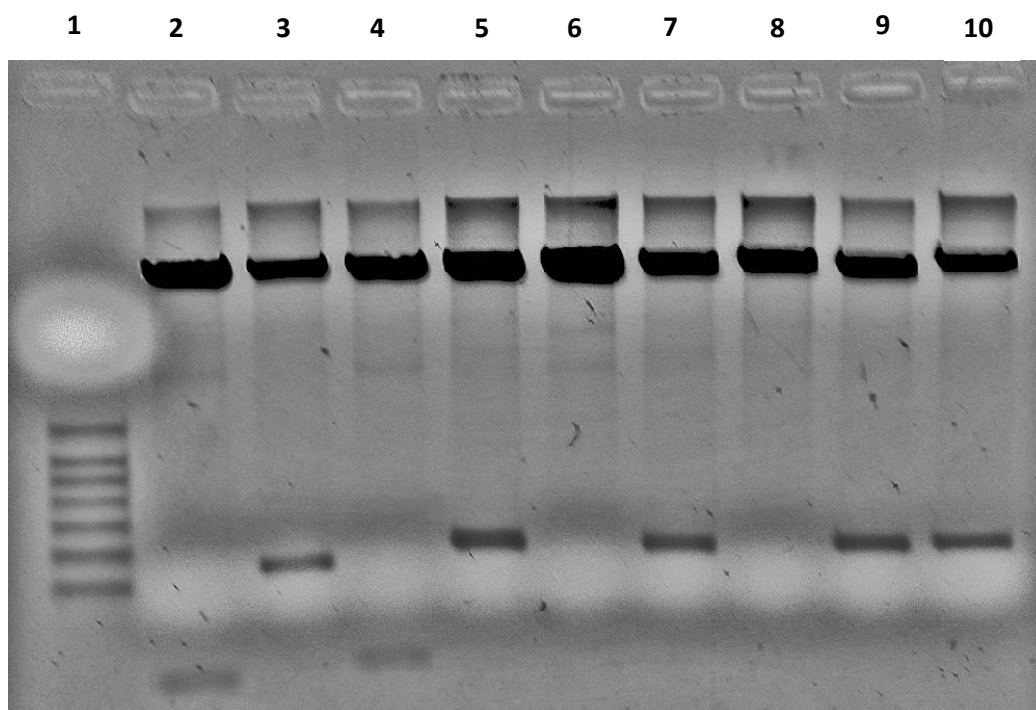
Fig 2C



Lane Descriptions: (1) 1 Kb ladder, (2) 300-1000 bp ladder, (3) empty, (4) *hoxb4a* plasmid #1 containing correct insert, (5) *hoxb4a* plasmid #2 containing correct insert, (6) *hoxb5a* plasmid #1 containing correct insert, (7) *hoxb5a* plasmid #2 containing correct insert.

Figure 2 (A-D): Digested Plasmid Gel Electrophoresis Images. 1.5% gel electrophoresis was performed following EcoRI restriction enzyme digestions of purified plasmids. The electrophoresis was performed to screen recombinant plasmids for the appropriate inserts. Lanes are numerically labeled, and descriptions are found below each image.

Fig 2D



Lane Descriptions: (1) 300-1000 bp ladder, (2) *hoxb5b* plasmid #1, (3) *hoxb5b* plasmid #2 containing correct insert, (4) *hoxb5b* plasmid #3, (5) *hoxb6a* plasmid #1 containing correct insert, (6) *hoxb6a* plasmid #2, (7) *hoxb6a* plasmid #3 containing correct insert, (8) *hoxb6b* plasmid #1, (9) *hoxb6b* plasmid #2 containing correct insert, (10) *hoxb6b* plasmid #3 containing correct insert.

Table 3: Purified Plasmid Quantifications

Purified Plasmid Name	Concentration (ng/ul)
b3b-c	132.6
c3a-b	47.9
c3a-c	74.2
a5a-c	107.9
b5b-2	65.1
b6a-1	89.3
b6a-3	82.6
b6b-3	82.2
b4a-1	113.1
b4a-2	145.6
b5a-2-1	83.4
b5a-2-2	113.5

Figure 3: Blast Information for Sequenced Plasmids

b3b

Sequences producing significant alignments:
(Click headers to sort columns)

Accession	Description	Max score	Total score	Query coverage	E value	Max ident
EF594314.1	Astatotilapia burtoni clone BAC 34I18 Hoxbb gene cluster, partial sequence	763	1145	100%	0.0	97%
EF594313.1	Astatotilapia burtoni clone BAC 116M8 Hoxaa gene cluster, partial sequence	97.1	97.1	18%	7e-21	81%
EF594312.1	Astatotilapia burtoni clone BAC 103K21 Hoxca gene cluster, complete sequence	95.3	95.3	21%	2e-20	79%
EF594310.1	Astatotilapia burtoni clone BAC 170E12 Hoxba gene cluster, complete sequence	54.7	54.7	4%	4e-08	100%

c3a

Sequences producing significant alignments:
(Click headers to sort columns)

Accession	Description	Max score	Total score	Query coverage	E value	Max ident
EF594312.1	Astatotilapia burtoni clone BAC 103K21 Hoxca gene cluster, complete sequence	455	703	99%	5e-129	99%
EF594314.1	Astatotilapia burtoni clone BAC 34I18 Hoxbb gene cluster, partial sequence	60.2	60.2	10%	5e-10	92%
EF594313.1	Astatotilapia burtoni clone BAC 116M8 Hoxaa gene cluster, partial sequence	60.2	60.2	14%	5e-10	85%

b4a

Sequences producing significant alignments:
(Click headers to sort columns)

Accession	Description	Max score	Total score	Query coverage	E value	Max ident
AB232920.1	Oryzias latipes hox gene cluster, complete cds, contains hoxBa, evx homologue	204	204	28%	5e-49	87%
AB207993.1	Oryzias latipes gene for hoxB4a, complete cds	204	204	28%	5e-49	87%

a5a

Sequences producing significant alignments:
(Click headers to sort columns)

Accession	Description	Max score	Total score	Query coverage	E value	Max ident
EF594313.1	Astatotilapia burtoni clone BAC 116M8 Hoxaa gene cluster, partial sequence	933	1017	99%	0.0	100%

b5a

Sequences producing significant alignments:
(Click headers to sort columns)

Accession	Description	Max score	Total score	Query coverage	E value	Max ident
EF594310.1	Astatotilapia burtoni clone BAC 170E12 Hoxba gene cluster, complete se	486	874	99%	2e-138	97%
EF594313.1	Astatotilapia burtoni clone BAC 116M8 Hoxaa gene cluster, partial seque	108	192	34%	2e-24	83%

b5b

Sequences producing significant alignments:
(Click headers to sort columns)

Accession	Description	Max score	Total score	Query coverage	E value	Max ident
EF594314.1	Astatotilapia burtoni clone BAC 34I18 Hoxbb gene cluster, partial seque	536	613	99%	2e-153	100%

b6a

Sequences producing significant alignments:
(Click headers to sort columns)

Accession	Description	Max score	Total score	Query coverage	E value	Max ident
EF594310.1	Astatotilapia burtoni clone BAC 170E12 Hoxba gene cluster, complete se	374	889	99%	2e-104	99%
EF594312.1	Astatotilapia burtoni clone BAC 103K21 Hoxca gene cluster, complete se	63.9	63.9	10%	4e-11	93%

b6b

Sequences producing significant alignments:
(Click headers to sort columns)

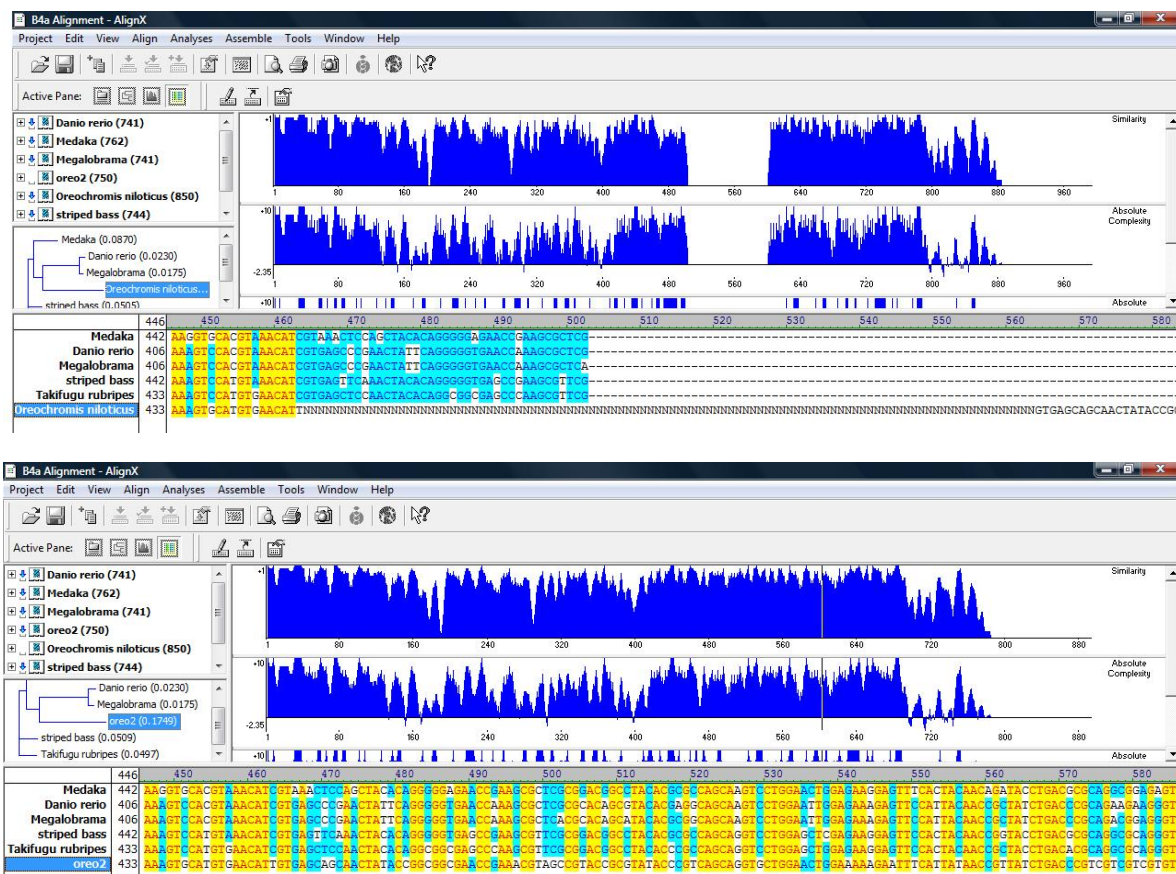
Accession	Description	Max score	Total score	Query coverage	E value	Max ident
EF594314.1	Astatotilapia burtoni clone BAC 34I18 Hoxbb gene cluster, partial seque	460	902	99%	1e-130	100%
EF594313.1	Astatotilapia burtoni clone BAC 116M8 Hoxaa gene cluster, partial seque	204	391	43%	2e-53	89%
EF594311.1	Astatotilapia burtoni clone BAC 150O18 Hoxab gene cluster, complete se	76.8	151	41%	5e-15	88%

Appendix Fig 3. Sequence data generated from dideoxynucleotide sequencing was entered into a Blast search to examine sequence identity.

Table 4: Insert Orientations

Gene Name	Forward Primer Strand Orientation
b3b	Plus/Plus
c3a	Plus/Plus
b4a	Plus/Plus
a5a	Plus/Minus
b5a	Plus/Plus
b5b	Plus/Plus
b6a	Plus/Minus
b6b	Plus/Plus

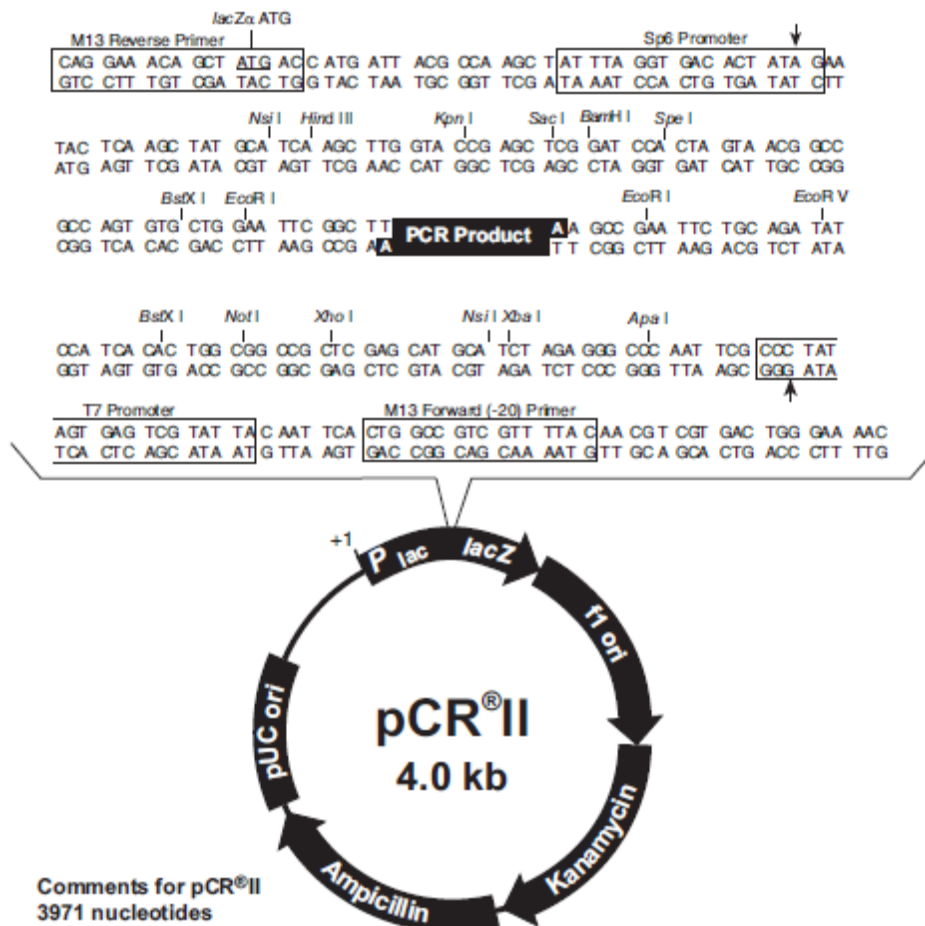
Figure 4: Multiple Species Alignment of the B4a Sequence



Multiple primer sets designed to amplify the *hoxb4a* gene for molecular cloning were unsuccessful in producing an amplicon of expected product size, and were typically non-specific as determined by multiple bands present in amplified genomic and cDNA despite optimized genomic conditions. The published partial coding sequence for *O. niloticus hoxb4a* included a 100 nucleotide expanse of unknown sequence (top). This anomaly would normally have been bypassed, using the *A. burtoni* published sequence for generation of primer sets. Ironically, the investigators who published the *A. burtoni* sequences were unable to isolate *hoxb4a* from their cDNA library.

In order to create working PCR primer sets for *hox B4a*, the *hoxb4a* sequence data for five related species was pulled and aligned with the published, flawed, *O. niloticus hoxb4a* sequence. Species used for the alignment included *Oryzias latipes*, *Danio rerio*, *Takifugu rubripes*, *Morone saxatilis*, and *Megalobrama amblycephala*. The alignment showed many areas of homology across the species. Intriguingly, after the experimental removal of the 100 bp expanse of unknown nucleotides in the *O. niloticus* partial cDNA sequence, the *O. niloticus hoxb4a* sequence was found to be very homologous with the consensus sequence for the overall alignment (bottom). In order to prevent designing primers based upon potentially poor *O. niloticus* sequencing information, primers were then designed using conserved regions of the alignments. The new primers were able to amplify a product of expected size.

Figure 5: Invitrogen's Dual Promoter pCRII Plasmid Map



LacZα gene: bases 1-587
 M13 Reverse priming site: bases 205-221
 Sp6 promoter: bases 239-256
 T7 promoter: bases 404-423
 M13 (-20) Forward priming site: bases 431-446
 f1 origin: bases 588-1025
 Kanamycin resistance ORF: bases 1359-2153
 Ampicillin resistance ORF: bases 2171-3031
 pUC origin: bases 3176-3849

Table 5: Solutions Prepared for Whole Mount *In Situ* Hybridization

0.1 % (v/v) DEPC-treated water: To 1 liter of Millipore water add 1 ml DEPC. Incubate at 37°C overnight, autoclave 121°C for 20 minutes. For volume superior to 1 liter adjust the DEPC volume and the autoclaving time appropriately.

Proteinase K: make up a stock solution of proteinase K at 20 mg/ml in 50 % glycerol, 10 mM Tris pH 7.8, and store in aliquot at -20°C.

Paraformaldehyde/PBS fixative (4% solution): 4 g paraformaldehyde is dissolved in PBS at 65°C. If it does not readily dissolve add a drop or two of 1 M NaOH solution to pH 7.5. It should be cooled to 4°C and used within 2 days.

PBS (Phosphate Buffer Saline) : (130 mM NaCl (), 7 mM Na₂HPO₄ 2H₂O, 3mM NaH₂PO₄ 2H₂O). For 10 X PBS mix 75.97 g NaCl, 12.46 g Na₂HPO₄ 2H₂O, 4.80 g NaH₂PO₄ 2H₂O. Dissolve in 800 ml DEPC-treated water, adjust to pH 7.0 and a final volume of 1 liter. Sterilize by autoclaving.

PBT: PBS, 0.1 % Tween-20. To 1 liter of DEPC-treated PBS add 1 ml of 20 % Tween.

Tween-20: (Fisher, cat number: BP337-200, lot number: 011560) make a 20% solution in DEPC-treated water. Store at room temperature

20 X SSC for hybridization and washing: (3 M NaCl, 300 mM tri-sodium citrate) Dissolve 175.3 g NaCl and 88.2 g sodium citrate in 800 ml of DEPC treated water. Adjust the pH with 1 M Citric Acid to 6.0. Adjust the volume to 1 liter and sterilize by autoclaving.

Pre-Hybridization Buffer: In a 50 ml tube mix the following reagents: 32.5 ml of Formamide, 12.5 ml 20 X SSC/DEPC, 25 µl Heparin (100 mg/ml), 250 µl 20 % Tween-20. pH to 6.0 with 1 M citric acid, adjust the volume to 50 ml with DEPC-treated water. Store the solution at -20°C.

Hybridization buffer: To 50 ml of the pre-hybridization buffer add 500 μ l of the Yeast tRNA solution. Keep at -20°C .

Heparin: make a stock solution of 100 mg/ml in DEPC treated distilled water. Store in aliquots at -20°C .

Yeast tRNA : dissolve in DEPC treated deionized water at 50 mg/ml. Store in aliquots at -20°C .

PI buffer: (PBT + 2% sheep serum + 2mg/ml Bovine Serum Albumin fraction V (stored at 4°C)). For 50mL: Add 1.0mL sheep serum (stored in 1mL aliquots at -20°C), 100 mg BSA to 49mL of PBT. Store in 10 ml aliquots at -20°C .

AP Buffer

Reactant	Initial Concentration	Volume	Final Concentration
Tris pH 9.5	2M	500 μ l	0.1M
MgSO ₄	1M	500 μ l	0.05M
NaCl	5M	200 μ l	0.1M
Tween 20	20%	50 μ l	0.10%
DEPC-H ₂ O		8.75 mL	

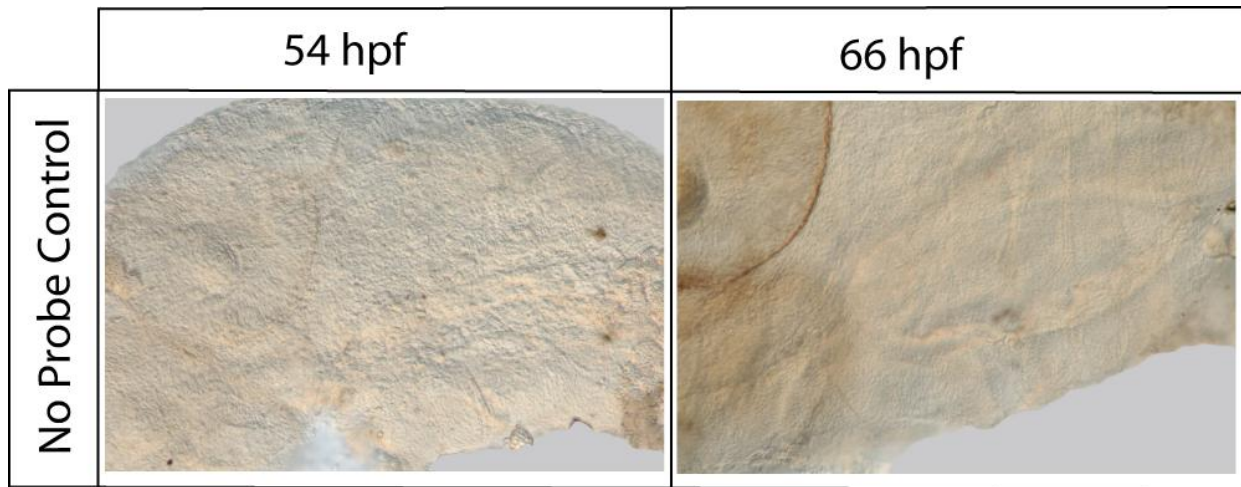
DIG/AP Development Buffer

Reactant	Initial Concentration	Volume	Final Concentration
Tris pH 9.5	2M	500 μ l	0.1M
MgSO ₄	1M	500 μ l	0.05M
NaCl	5M	200 μ l	0.1M
Tween 20	20%	50 μ l	0.10%
DEPC-H ₂ O		8.75 mL	

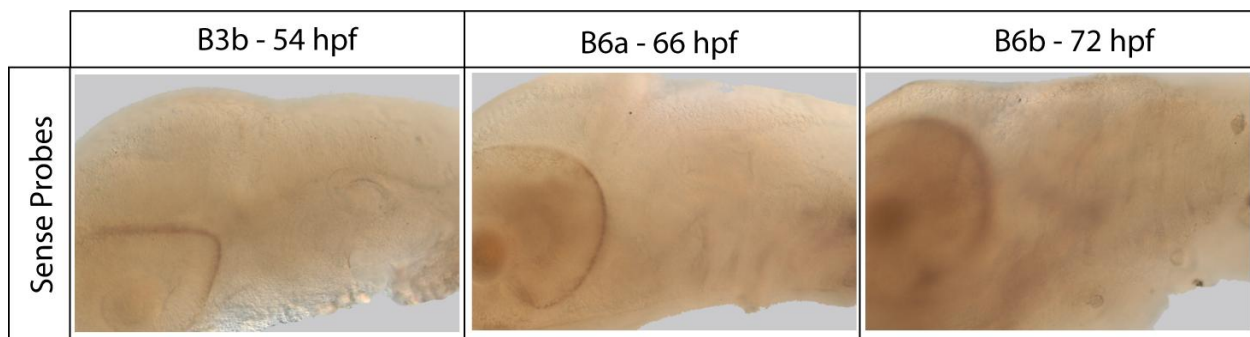
After the solution is mixed, add 4 mg NBT and 2 mg BCIP. Protect from light.

APPENDIX B:
Additional Images from Whole Mount *In Situ* Hybridization

No Probe (Negative Control)

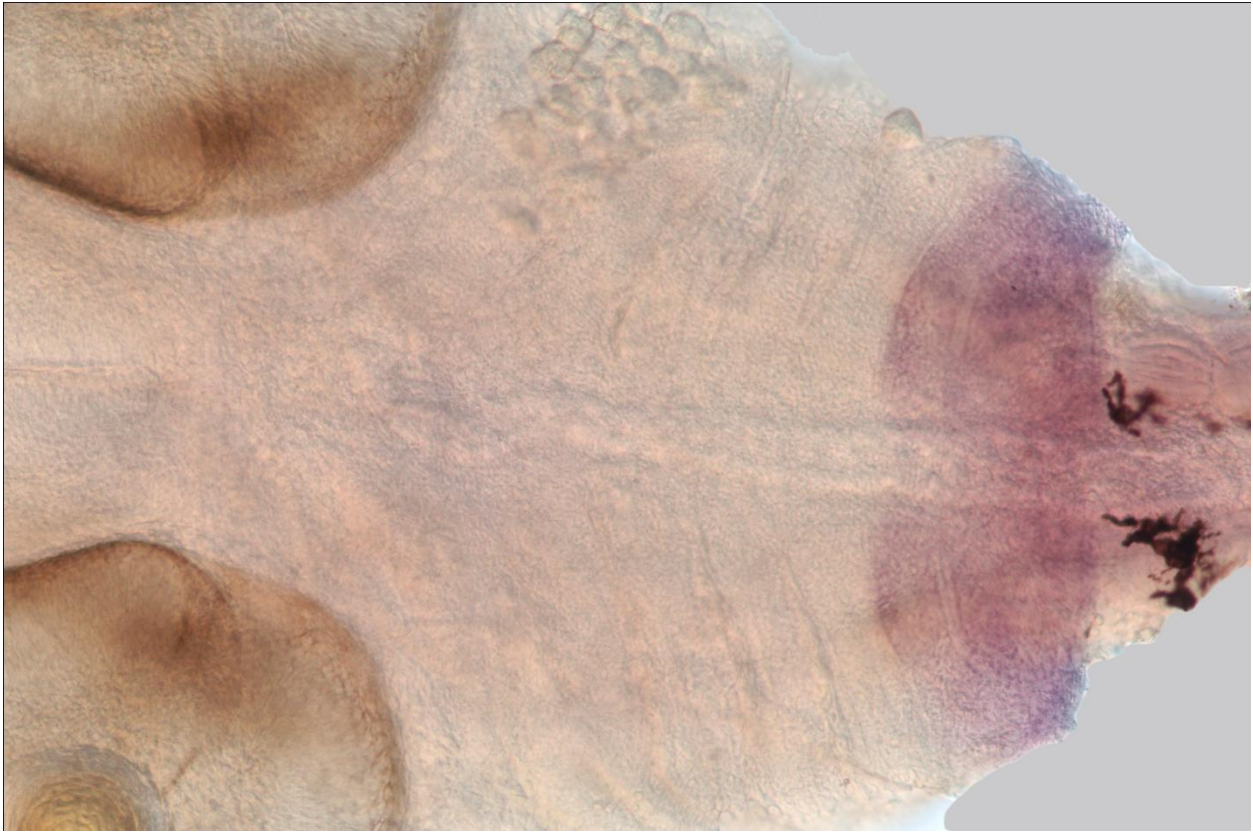


Selected Images of Sense Probes (Negative Control)



Negative control *in situ* hybridizations were performed in Nile tilapia embryos as shown. All specimens are shown with dorsal to the top, anterior to the left. TOP-images obtained from a “no probe” *in situ* hybridization. BOTTOM-Representative images from *in situ* hybridizations utilizing sense strand riboprobes, indicating no nonspecific hybridization of probe to mRNA.

Ventral Mount
Hoxa5a – 72 hpf



Pharyngeal expression of the *hoxa5a* gene in Nile tilapia embryos at 72 hpf. The specimen is mounted in a ventral position with the anterior to the left. *Hoxa5a* expression is observed in PA 6-7 at 72 hpf as well as within the anterior neural tube.

APPENDIX C:
Approval of Research Involving Animals



Animal Care and Use Committee
East Carolina University
212 Ed Warren Life Sciences Building
Greenville, NC 27834
252-744-2436 office • 252-744-2355 fax

November 7, 2007

Jean-Luc Scemama, Ph.D.
Department of Biology
Howell Science Complex
East Carolina University

Dear Dr. Scemama:

Your Animal Use Protocol entitled, "Investigation of the Evolutionary Role of the Major Genes Responsible for Patterning the Jaw Apparatus of the Nile Tilapia," (AUP #D198a) was reviewed by this institution's Animal Care and Use Committee on 11/7/07. The following action was taken by the Committee:

"Approved as submitted"

A copy is enclosed for your laboratory files. Please be reminded that all animal procedures must be conducted as described in the approved Animal Use Protocol. Modifications of these procedures cannot be performed without prior approval of the ACUC. The Animal Welfare Act and Public Health Service Guidelines require the ACUC to suspend activities not in accordance with approved procedures and report such activities to the responsible University Official (Vice Chancellor for Health Sciences or Vice Chancellor for Academic Affairs) and appropriate federal Agencies.

Sincerely yours,

A handwritten signature in black ink, reading 'Robert G. Carroll, Ph.D.'.

Robert G. Carroll, Ph.D.
Chairman, Animal Care and Use Committee

RGC/jd

enclosure